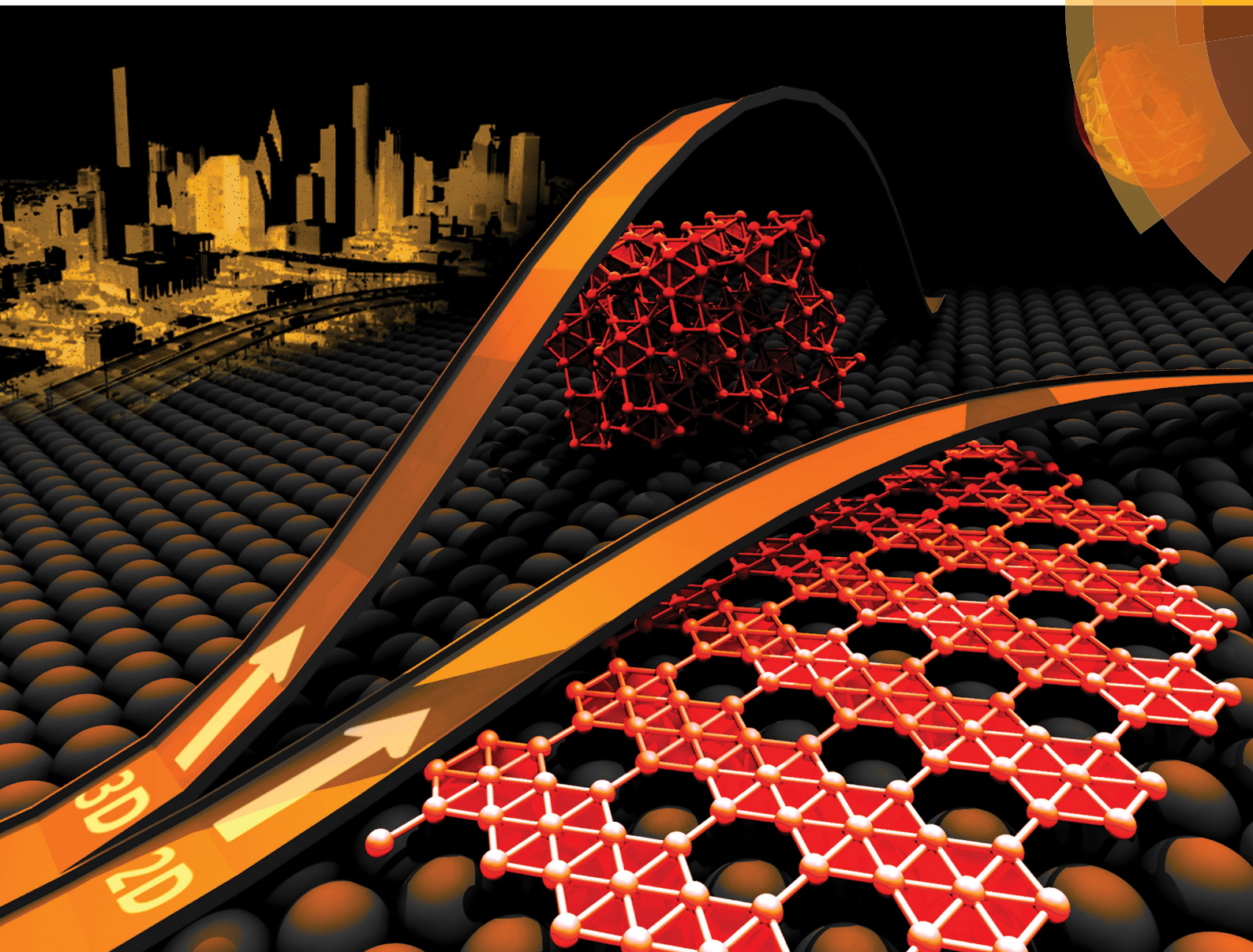


Chem Soc Rev

Chemical Society Reviews

rsc.li/chem-soc-rev



ISSN 0306-0012



ROYAL SOCIETY
OF CHEMISTRY

REVIEW ARTICLE

Boris I. Yakobson *et al.*

Two-dimensional boron: structures, properties and applications



Cite this: *Chem. Soc. Rev.*, 2017, 46, 6746

Two-dimensional boron: structures, properties and applications

Zhuhua Zhang,^{id} ^{ab} Evgeni S. Penev^{id} ^b and Boris I. Yakobson*^{bc}

Situated between metals and non-metals in the periodic table, boron is one of the most chemically versatile elements, forming at least sixteen bulk polymorphs composed of interlinked boron polyhedra. In low-dimensionality, boron chemistry remains or becomes even more intriguing since boron clusters with several to tens of atoms favor planar or cage-like structures, which are similar to their carbon counterparts in terms of conformation and electronic structure. The similarity between boron and carbon has raised a question of whether there exists stable two-dimensional (2D) boron, as a conceptual precursor, from which other boron nanostructures may be built. Here, we review the current theoretical and experimental progress in realizing boron atomic layers. Starting by describing a decade-long effort towards understanding the size-dependent structures of boron clusters, we present how theory plays a role in extrapolating boron clusters into 2D form, from a freestanding state to that on substrates, as well as in exploring practical routes for their synthesis that recently culminated in experimental realization. While 2D boron has been revealed to have unusual mechanical, electronic and chemical properties, materializing its potential in practical applications remains largely impeded by lack of routes towards transfer from substrates and controlled synthesis of quality samples.

Received 11th April 2017

DOI: 10.1039/c7cs00261k

rsc.li/chem-soc-rev

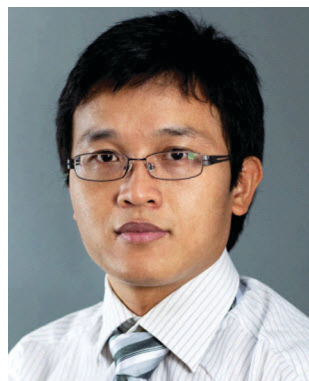
^a State Key Laboratory of Mechanics and Control of Mechanical Structures, and Key Laboratory for Intelligent Nano Materials and Devices of Ministry of Education, Nanjing University of Aeronautics and Astronautics, Nanjing 210016, China

^b Department of Materials Science and NanoEngineering, Rice University, Houston, TX 77005, USA

^c Department of Chemistry, Rice University, Houston, TX 77005, USA.
 E-mail: biy@rice.edu; Tel: +1 713-348-3572

1. Introduction

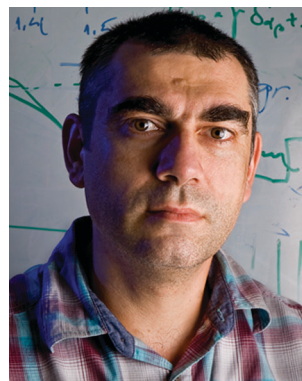
Ignited by the discovery of novel physics in graphene, two-dimensional (2D) materials beyond graphene have gained unprecedented interest across materials research. While graphene-like 2D materials have been reported to be rich and diverse, only a small number of them are mono-elemental, such as phosphorene,



Zhuhua Zhang

Prof. Zhuhua Zhang obtained his BE degree in 2004 and completed his PhD research with Prof. Wanlin Guo in 2010, both at Nanjing University of Aeronautics and Astronautics, China. As a postdoctoral fellow, he joined Prof. Yakobson's group in the Department of Materials Science and NanoEngineering at Rice University in May 2012. With the support of the Thousand Talent Program of China, he started a theoretical group at

Nanjing University of Aeronautics and Astronautics from May 2017. His current research interests include modulation of structures and properties of low-dimensional materials, nanomechanics as well as computational design of novel nanostructures.



Evgeni S. Penev

Evgeni S. Penev is an assistant research professor at Rice University. He studied physics at the St. Clement of Ohrid University of Sofia, Bulgaria, and holds a MS degree in solid state physics. He received his PhD degree from the Fritz Haber Institute of the Max Planck Society, Germany, and was awarded the Otto Hahn Medal for outstanding scientific achievement.

silicene, germanene and stanene.¹ More surprising is the fact that none of these elemental 2D materials possesses structural planarity as in graphene, due to their varying degrees of out-of-plane buckling. The reason is that all these elements have very limited ability in varying their bonding nature, unlike carbon which is able to variably form sp^3 , sp^2 and sp bonding. This fact has kept researchers pondering whether there is an element that could be on par with carbon in bonding variability and thereby form a purely flat 2D material. As the $Z - 1$ ("left") neighbor of carbon in the periodic table, boron is similar to carbon in terms of electronic properties and potential applications in, for example, superhard materials² and biological compounds.³ However, boron is still among the most mysterious elements due to its complicated chemistry, despite the long history of boron research and the fact that very few elements can be simpler than this light atom.^{4,5}

The study of boron can be traced back to two centuries ago,^{6,7} when boron only existed in various compounds due to its unusual ability to combine with almost all other elements. Pure boron was not documented until Sands' work in 1957,⁸ which reported bulk γ -B₁₀₆ with an extremely complex structure. Nowadays, bulk boron is known to have at least sixteen polymorphs, but only a few of them have crystal structures identified,^{9,10} all featuring interlinked polyhedra. Positioned between metallic beryllium and non-metallic carbon, boron has only three valence electrons: $[He]2s^22p^1$. The single 2p electron would favor metallicity, but its orbital radius is close to that of the 2s state,¹¹ making it sufficiently localized to allow for the appearance of non-metallicity. Such a unique electronic structure of boron enables the formation of highly diverse bonding in bulk phases, ranging from strongly covalent two-centre bonds to metallic-like multi-centre bonds. The latter are responsible for the polyhedra, dominant in bulk boron (Fig. 1, top left inset), especially for the B₁₂ icosahedra¹² that can accommodate the electronic deficiency of boron.

The strong bonding capability of boron stimulated an upsurge of research interest in boron nanostructures, which include zero-dimensional (0D) clusters, 1D nanotubes and 2D

monolayer sheets (Fig. 1). Both theoretical and experimental studies have shown that small boron clusters, B_n, tend to adopt planar conformations in their ground state, whose electronic structures are markedly similar to those of aromatic or anti-aromatic molecules.^{13–19} As the cluster size increases, cage-like conformations start to compete in energy with the planar ones and become increasingly more favorable when the size exceeds a critical value ($n \sim 28$ at charge neutrality).²⁰ One prominent example of boron cages is the experimentally reported fullerene-like B₄₀ cluster, which proves to be the ground state among the 40-atom conformations by global minimum search.²¹ Actually, the research of boron cages has been boosted more by an earlier prediction of a B₈₀ buckyball,²² which remains a subject of particular interest in theory to date. The B₈₀ buckyball is iso-electronic to a C₆₀ buckyball, and its symmetry^{23,24} and stability relative to other proposed hollow or filled isomers^{25–30} have been intensely debated. While the B₈₀ buckyball turns out to be less stable than some isomers, unfolding it³¹ onto a plane can uniquely lead to the prediction of a stable flat crystal (Fig. 1), called an α -sheet,^{32,33} particularly appealing as a graphene analogue. The prediction of the α sheet further extended the similarities between boron and carbon chemistry and brought the research of boron into the vigorously explored materials flatland.

Despite the striking similarities between boron and carbon, 2D boron layers are made of a triangular grid with a pattern of hollow hexagons (HHs) (Fig. 1), distinctly different from graphene's honeycomb lattice. The HH pattern is highly variable in distribution and concentration, setting apart numerous lattices within a narrow range of energies near the ground-state line and resulting in polymorphism.³⁴ Searching for energetically favorable boron sheets encounters a daunting combinatorial problem and thus necessitates a large number of costly (energy) computations. The configurational space of 2D boron has been explored using different global minimum search methods, such as the particle swarm optimization,³⁵ advanced cluster expansion methods,³⁴ and evolutionary algorithms.³⁶ Yet, reaching the real global minimum of 2D boron is still subject to the development of more efficient methods that would make structures with larger unit cells feasible. Another salient difference from known 2D materials is that boron is remarkably higher in energy than its bulk forms, unlike graphene and h-BN sheet³⁷ that are naturally layered in 3D form. How to entice the boron atoms to assemble into metastable 2D structures proves to be a challenge, albeit experimental efforts intensified for nearly a decade. To this end, several theoretical studies^{38,39} have suggested using metal substrates, such as Ag and Cu, to lift the polymorphic energy degeneracy and kinetically guide the growth of boron sheets.

Benefiting from theoretical predictions, two recent experiments have independently realized monolayer boron sheets on Ag(111) substrates,^{40,41} which are one-atom thick and indeed polymorphic. Previously predicted metallic character^{32,34} of boron sheets is also confirmed experimentally⁴² and renders them a desirable complement to semimetallic graphene, insulating h-BN, and semiconducting transition metal dichalcogenides. These milestones highlight the power of theory in leading



Boris I. Yakobson

Boris I. Yakobson is the Karl F. Hasselmann Chair in Engineering, a professor of materials science and nano-engineering, and a professor of chemistry at Rice University, USA. He received his PhD degree in 1982 from the Russian Academy of Sciences, Russia. Prior to joining Rice in 1999, Yakobson was on the physics faculty at North Carolina State University and a visiting scholar at the Department of Chemistry, Columbia University, in 1990.

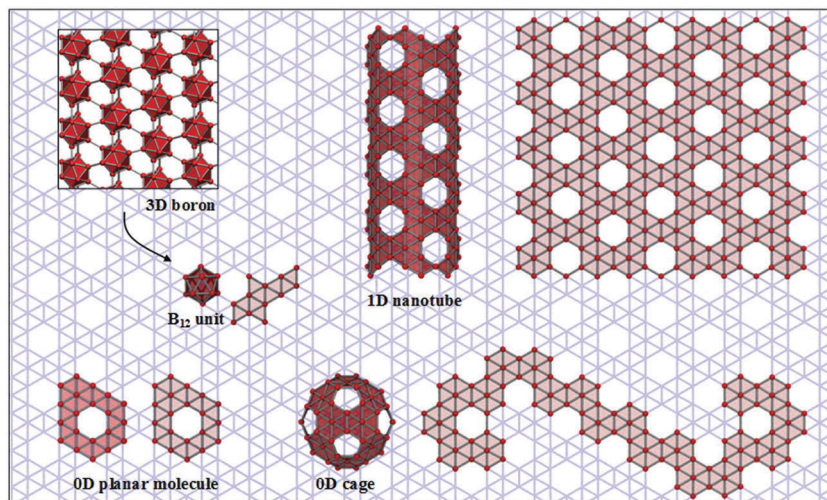


Fig. 1 The conceptual-geometrical precursor of the diverse boron structures. Two-dimensional (2D) boron monolayer can be cut-tailored into planar boron clusters, rolled into 1D nanotubes, and wrapped up into 0D boron fullerene. It can even be folded into a B_{12} cluster, the dominant building block of 3D boron (the inset shows the structure of 3D-bulk α -boron).

to synthesis of new materials and uncovering new properties and phenomena.^{43–45} Also, this progress has promptly raised broad interest in exploring the versatile properties and potential applications of borophenes. However, towards realizing practical applications, the separation of borophenes from substrates and controlled synthesis of quality samples remain challenging, calling for continuing synergy between theory and experiment.

In this review, we present the recent theoretical and experimental progress in low-dimensional boron structures, particularly focusing on borophene. We first discuss boron clusters, both compact 3D-cages and 2D-planar varieties. Then, we provide an extensive account of structural and electronic characteristics of 2D boron in vacuum and on substrates and highlight the role of theory in locating favorable structures of boron sheets in different environments and in guiding experimental synthesis. The experimental advances in synthesizing and characterizing borophenes are then surveyed and possible directions for future study are analyzed. Finally, we summarize the current state of the studies of mechanical, electronic and chemical properties of borophenes as well as their prospective applications in relevant technological fields.

2. Boron clusters

The actively explored boron clusters, B_n , normally refer to those with n varying from 3 to ~ 100 atoms. A crucial first step in theoretically studying boron clusters is to identify their global energy minima. Yet, as n increases, each boron cluster would have an exponentially growing number of possible isomers due to a rich variety of B–B bonds. Many research groups have developed global minimum search methods based on different algorithms, including gradient embedded genetic algorithm,⁴⁶ coalescence kick,⁴⁷ basin hopping,⁴⁸ Cartesian walk,⁴⁹ particle

swarm optimization,³⁵ genetic/evolutionary algorithms,^{50–52} data mining methods,^{53,54} *etc.* Combining these methods with density functional theory (DFT) calculations, theory could identify the ground state structures of a set of boron clusters, most of which have been detected experimentally. Details of these structural search methods and their respective advantages have been summarized in recent reviews,^{13,15} thus not further discussed here.

While bulk boron phases favor inter-linked polyhedra, small boron clusters tend to adopt planar structures (Fig. 2a), typically consisting of a periphery and interior boron atoms. All bonds around the periphery are classical two-centre two-electron bonds (two electrons shared by two atoms) while those for the interior atoms are delocalized multi-center two-electron bonds (two electrons shared by three atoms or more). The planar conformation of small boron clusters could be rationalized by the aromaticity or antiaromaticity of the delocalized molecular orbitals, similar to the electronic structures of aromatic molecules. For discussion on the bonding configurations in planar boron clusters, we refer the reader to several comprehensive reviews.^{13,14} As the cluster size increases, the bonds around the periphery become shorter than those in the interior, squeezing the inner boron atoms slightly out of the plane and resulting in quasi-planar structures, *e.g.*, B_7^- (ref. 55) and B_{12}^- .⁵⁶ With further increasing the cluster size, a 2D \rightarrow 3D structural crossover occurs at $n = 20$, at which a double-ring tubular isomer (see insets in Fig. 2) can compete with the planar structure in terms of stability, as confirmed by global minimum search in conjunction with photoelectron spectroscopy (PES) characterization.⁵⁷ The appearance of tubular boron clusters has stimulated interest as they can be considered as embryos of boron nanotubes. However, the tubular cluster turns out to be high in energy at larger size, at least according to results from state-of-the-art DFT calculations.

Even though favorable ring-like clusters have not been further identified, fullerene-like boron cages can be favorable

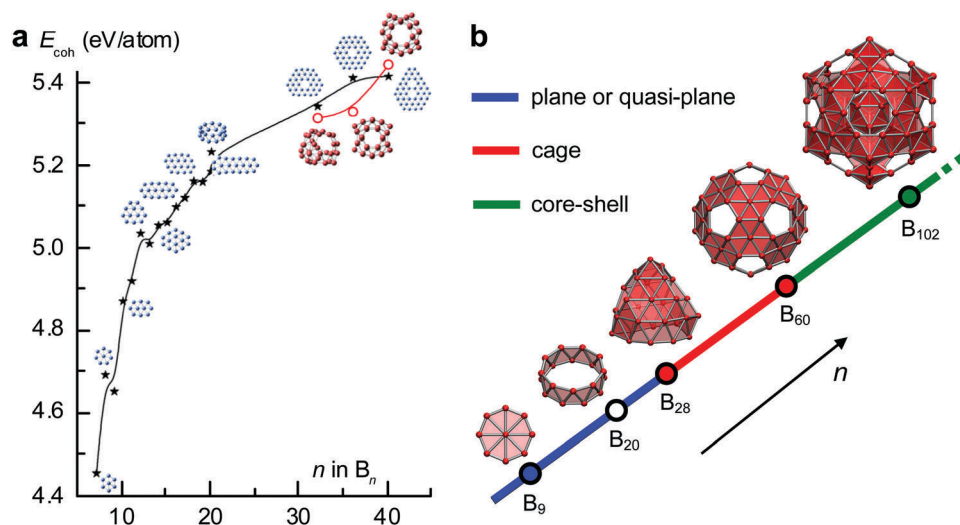


Fig. 2 Structures and stability of boron clusters. (a) Cohesive energies per atom for B_n ($n = 7-40$) clusters at charge-neutral state, calculated using PBE0 functional. The black stars stand for the (quasi-) planar or double-ring tubular ($n = 20$) structures while the red circles stand for the cage structures ($n = 32, 36$ and 40). (b) Size-dependent conformation of favorable boron clusters: from planar or quasi-planar, via cage-like, to core-shell structures.

when $n \geq 28$ ^{58,59} (Fig. 2). Structurally, the fullerene-like cages can reduce the edge energy at the expense of bending energy, which decreases with increasing n . The fact that boron cages at specific sizes can satisfy an electron-counting rule for spherical aromaticity further improves their stability over the planar form. The most remarkable example is the recently reported B_{40} cage,²¹ which is significantly more stable than its planar isomers at the charge-neutral state. It is unusual that the B_{40} cage has no pentagon normally required for a spherical structure. Instead, its surface exhibits four hollow heptagons, which would generate a negative Gaussian curvature in a graphene-like lattice. This peculiar cage structure raises a question as to what is its geometrical precursor.^{60,61} In contrast, one of its larger siblings, the B_{80} buckyball,²² has a more regular spherical structure composed of pentagons and hexagons, reminiscent of a C_{60} fullerene that shares the same icosahedral symmetry. Despite presently remaining hypothetical and the fact that several more stable isomers have been proposed,²⁵⁻³⁰ the B_{80} buckyball can be directly unfolded into an energetically favorable boron sheet, referred to as an α -sheet, as will be discussed later. It is worth mentioning that hollow structures of these boron cages can trap metal atoms to form various endohedral metallofullerenes with novel magnetic^{62,63} and chemical⁶⁴ properties. Further studies of large boron clusters ($n \geq 80$) revealed that they would develop into core-shell structures (often with a B_{12} icosahedron core, see Fig. 2b),^{25,27,30} showing a tendency of converging to bulk boron lattices.

Aside from the size, the competition between the stability of planar and cage-like boron structures also depends on their charge state. For example, a planar B_{40}^- structure is lower in energy than the B_{40}^- cage structure, which otherwise is the ground state at charge-neutrality.²¹ A similar relation also occurs in other boron clusters charged by one electron, such as B_{28}^- (ref. 58) and B_{29}^- .²⁰ It appears that, for a number of boron clusters, a planar geometry is preferred at the -1 anion state

while a cage structure is more favorable at charge-neutrality. The charge-dependent structure of boron clusters opens the possibility for their structural control, as recently shown for 2D boron monolayers.⁶⁵

With increasing size, both the planar and cage-like boron clusters tend to contain hollow hexagons. The smallest planar cluster featuring such a HH is B_{27}^- .⁶⁶ As the size increases further, clusters with HHs become increasingly more stable than the isomers without HHs. The planar B_{36} cluster¹⁷ contains a perfect HH and has the same six-fold symmetry as graphene, which can be viewed as a basic unit for constructing the α -sheet. The planar B_{40}^- cluster contains a twinned HH²¹ (see the inset in Fig. 2a), which also appears often in the boron sheets with high HH concentrations.³⁴ Larger planar clusters should show a richer variety of HH patterns. A similar trend holds for the fullerene-like clusters. The more favorable HHs in larger boron clusters are indeed reminiscent of the vacancy-rich structures of stable 2D boron sheets.³²⁻³⁴

On the experimental side, the current method for synthesizing boron clusters is mainly through laser evaporation of boron targets, such as boron rods, similar to early fullerene making. The vaporized atoms are then cooled to form clusters of various sizes, and the cluster of a certain size can be selected by a mass gate. Identification of cluster structures has been carried out primarily through PES,⁶⁷ which is compared to PES spectra obtained from DFT calculations. While good agreement between experimental and theoretical PES spectra can be achieved for most of the reported boron clusters, there is still no direct imaging of their atomic structures. The challenge lies in the fact that the produced boron clusters are in the gas phase and prone to aggregation upon decreasing the temperature, making microscope-imaging impossible. Controllable synthesis of boron clusters with selected size and then depositing them onto an inert substrate would be the first step towards obtaining atomic-resolution images.

3. Borophenes

3.1 Freestanding borophene

Since the discovery of graphene,⁶⁸ many elements and blends have been shown to form 2D materials. Boron nitride,^{69,70} transition metal dichalcogenides,^{71,72} phosphorus,⁷³ silicon^{74,75} and tin^{76,77} have been actively studied in this realm, yet few of them can compete with boron in terms of chemical similarity to carbon. Hence, intriguing questions arise: can boron form a 2D material as carbon does in the form of graphene? If so, what are the energetically preferred structures of 2D boron? The first tentative 2D boron structure is borrowed from graphene, *i.e.*, a hexagonal sheet with boron atoms arranged in a honeycomb network. The graphitic boron layer naturally exists in a group of transition metal diborides and was predicted to be favorable on the (0001) surfaces of NbB₂,⁷⁸ CrB₂ and MoB₂⁷⁹ under boron rich conditions. Such a honeycomb boron layer was originally named “boraphene”,⁷⁸ but it is unstable in the freestanding form since boron lacks one electron to form stable sp² hybridization.^{80,81} Inspired by the prevalence of hexagonal boron pyramids in quasi-planar boron clusters,^{82,83} Boustani argued, by invoking the Aufbau principle, that the most stable 2D boron would be composed of buckled triangular motifs.⁸⁴ Such a buckled triangular sheet was later found to be the most stable among several hand-designed sheet configurations⁸⁵ and was once used as a precursor to construct boron nanotubes,^{86,87} reported once as apparently synthesized, several years earlier.^{88,89} Advances in the theoretical studies of 2D boron structure were made by Tang *et al.*³² and Yang *et al.*,³³ who independently proposed the boron α -sheet, derived by unfolding the B₈₀ buckyball onto a plane. The α -sheet is composed of triangular lattice patterned by isolated HHs, with a D_{6h} symmetry. As an electronic equivalent of graphene, the α -sheet is more stable by 37 meV per atom than the buckled triangular sheet. Its high stability is explained by an optimal filling of in-plane electronic orbitals,³² which also accounts for its flat conformation. Subsequently, Tang *et al.* proposed several boron sheets by arranging the HHs in different patterns and concentrations and found that several of them have cohesive energies as good as that of the α -sheet.⁹⁰ This result opens a broader question about the possible polymorphism of 2D boron.

Searching for the lowest energy structure becomes a focus of subsequent studies of 2D boron. As there are numerous possibilities for arranging HHs (denoted as [] for the vacant sites) in a triangular grid (B), direct use of DFT methods for calculating every possible structure is unrealistic. To evaluate the structural stability and diversity, Penev and coworkers³⁴ treated the boron sheet as a pseudo-alloy B_{1- ν][ν], where the HH concentration is defined as $\nu = m/N$, with m the number of HHs in a supercell of N triangular lattice sites. Then any boron sheet can be described by a vector σ , with components $\sigma_i = +1$ for the hexagon center where a B atom is present and -1 if not. For a particular configuration σ , the total energy E can be expanded in series}

$$E(\sigma) = J_0 + (1 - 2\nu)J_1 + \sum d_x J_x \Pi_x(\sigma), \quad (1)$$

where d_x is the number of clusters of type x , which can be pairs, triplets, *etc.*, J_x is the corresponding effective cluster interaction, and $\Pi_x(\sigma) = \langle \prod_i \sigma_i \rangle$ represents the “spin” products for configuration σ averaged over all symmetry-equivalent x -type clusters. This treatment allows for the use of the cluster expansion method⁹¹ augmented with accurate DFT calculations to determine the expansion coefficients J_x and then to more easily explore the configurational space of 2D boron. All the calculated symmetry-inequivalent structures are depicted in Fig. 3a, where the 2D boron is shown to be inherently polymorphic, with all stable isomers lying in a narrow range of HH concentrations of 10–15%. In particular, the $\nu_{1/8}$ and $\nu_{5/36}$ sheets are slightly more stable than the α -sheet ($\nu = 1/9$). Later on, employing different global-optimization methods, more theoretical studies^{92–94} have further extended the search for new isomers. All their results confirmed the polymorphism of 2D boron, even though the ground states may differ slightly from calculations using different functionals.

Based on the structure–stability relationship set forth above, a stabilizing mechanism for the boron sheets can be proposed.⁹⁵ In a boron sheet, the B atoms at the center of hexagons serve as “donors” while the HHs act as “acceptors”,⁹⁶ which are mixed to compensate for the electronic deficiency of boron. If three valence electrons of each “donor” boron were fully shared with the hexagonal skeleton (colored in grey, inset of Fig. 3a), an ideal boron sheet should have the skeleton isoelectronic to graphene. This simple mechanism explains why the $\nu_{1/9}$ sheet is one of the most favorable structures. Including some secondary factors, such as the vacancy–vacancy interaction (*e.g.*, such an interaction is enhanced in twinned vacancies), could shift the ground state structure to a slightly higher ν ($\sim 1/8$), which then achieves good agreement with DFT calculations. The boron sheets with $\nu < 1/9$ are electron-excessive and exhibit off-plane buckling due to mixing of in-plane and out-of-plane orbitals, whereas those sheets with $\nu > 1/9$ are purely flat, as shown in Fig. 3c. The boron sheet with a high ν is electron-deficient and tends to draw electrons from its surroundings, so as to stabilize its structure. An extreme example is the hexagonal boron sheet ($\nu = 1/3$), which is unstable in a vacuum yet at the global minimum in many bulk metal diborides due to electron transfer from the metal layers.⁷⁹

3.2 Boron nanostructures on substrates

In contrast to other 2D materials (*e.g.*, graphene, h-BN, and MoS₂) that are naturally layers stacked in the ground-state 3D forms, 2D boron is far higher in energy than all its 3D forms (Fig. 4a). For example, the α -sheet is less stable by 400 meV per atom than bulk α -boron. The thermodynamic disadvantage of 2D boron, together with its inherent polymorphism, leads to a significant challenge for its synthesis. Prior to experimental efforts, theoretical studies are instrumental in shedding light on several fundamental questions that hamper the synthesis.

Nucleation of 2D boron. The first question is what can entice boron atoms to assemble into 2D structures. An idea is that the nucleation barriers for 2D or 3D, controlling the material formation, do not need to always rank in the same order as the

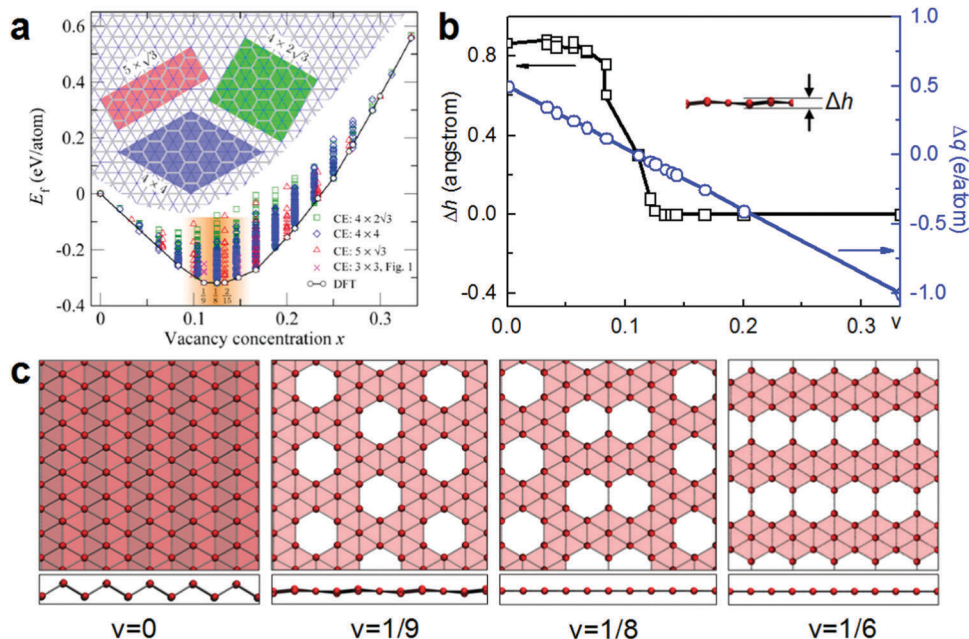


Fig. 3 Stability and structures of 2D boron. (a) Total energy per atom of all symmetry-inequivalent B sheets as a function of v . Diamonds show the data expanded using a rhombus primitive cell while squares show those expanded from a rectangular primitive cell as shown in the inset, both with the cluster expansion method. The solid line shows the energy variation of ground states with v . Reprinted with permission from ref. 34. Copyright 2012 American Chemical Society. (b) Black line: the buckling magnitude of favorable B sheets as a function of v . Blue line: the dependence of excessive electrons (see text for definition) per atom in the honeycomb boron lattice (grey in the inset of a) with respect to the number of valence electrons per carbon atom in graphene. (c) Front and side views of atomic structures of the triangular, $v_{1/9}$, $v_{1/8}$ and $v_{1/6}$ sheets.

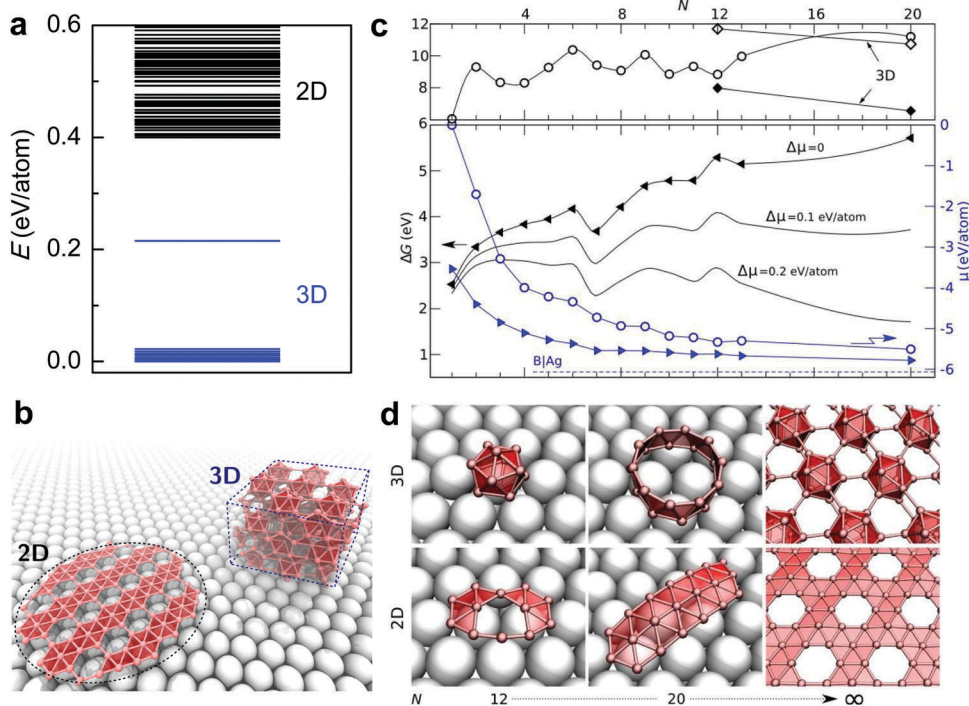


Fig. 4 2D versus 3D boron on metal substrate. (a) Energy comparison between 2D boron sheets and bulk boron in a vacuum. (b) A 2D boron nucleus has all atoms interacting with the metal while only atoms on one surface of a 3D boron nucleus interact with the metal. (c) Upper: Free energy variation of 2D (line with circle) and 3D (line with diamond) boron clusters on Ag as a function of number of B atoms, N . Bottom: Formation energy of 2D boron clusters and chemical potential of boron as functions of N . (d) Representative atomic structures of favorable 3D and 2D boron clusters on Ag, with $N = 12$, 20 and ∞ .

energies of final phases. A further control knob can be borrowed from the CVD synthesis of graphene or h-BN, namely using a metal substrate. All n atoms of a 2D-nucleus can benefit from the interaction with the substrates while only $\sim n^{2/3}/6$ atoms in a 3D-nucleus can be in contact with the substrate (Fig. 4b). In this manner, the substrate can selectively stabilize 2D structures, suppressing the nucleation barrier to be lower than that for the 3D case. Once the 2D route is preferentially chosen, the boron structures can be kinetically protected from converting into 3D form. This scenario is supported by atomistic calculations performed by Liu *et al.*,³⁹ who indeed found a smaller nucleation barrier for the 2D route than that for the 3D route (Fig. 4c and d). Their results also confirmed that planar clusters are more favorable than the 3D clusters (Fig. 4d), at least for B_n with $n \leq 20$ on Ag(111). Based on DFT computations, they suggested two potential routes towards the synthesis of 2D boron: (i) deposition of boron sources on the Au or Ag surface, (ii) saturation of B-terminated MgB_2 surfaces in a boron-rich environment. Liu, Gao and Zhao⁹⁷ also investigated favorable geometries and the interaction mechanism of boron clusters on Cu(111) and found that HHs can easily form during the nucleation of 2D clusters, further supporting the viability of using metal substrates to assist the synthesis of 2D boron.

2D boron on metals. While metal substrates are necessary for the growth of 2D boron, the metal–boron interaction may alter its ground-state structure in view of the high structural

sensitivity of borophenes to charge doping.^{65,96,98} The structures of 2D boron predetermined by metal substrates will serve as a basis for any further study of this material. Thus, another fundamental question is what structures will be favored on metals. While the search for the global minimum of freestanding 2D boron has been performed well, including metal substrates into the search will make the tasks computationally much more taxing. Recently, Zhang *et al.*³⁸ employed the cluster expansion method, including explicitly the metal substrate, while still treating the boron–metal system as a “binary alloy”³⁴ composed of a triangular boron lattice and HHs, both supported on a metal substrate. This treatment enables a comprehensive first-principles study of 2D boron on metals commonly used in CVD synthesis. The results show that 2D boron is the first material whose favorable structure depends on substrates (Fig. 5a). In particular, Ag, Cu and Ni donate electrons into 2D boron and hence increase the HH concentration, which, along with the potential provided by the substrate, results in the $\nu_{1/6}$ sheet as the ground state. This trend agrees with the fact that a graphitic boron layer can be the ground state on (0001) surfaces of metal diborides,^{78,79} where electronic transfer from the metal layers makes the boron electronically equivalent to carbon. In contrast, electrons are drawn from boron by Au, which shifts the ground state of 2D boron toward a smaller ν value and preserves its structural degeneracy as in a vacuum (Fig. 5b and c). Remarkably, the predicted optimal $\nu_{1/6}$ sheet on Ag(111)

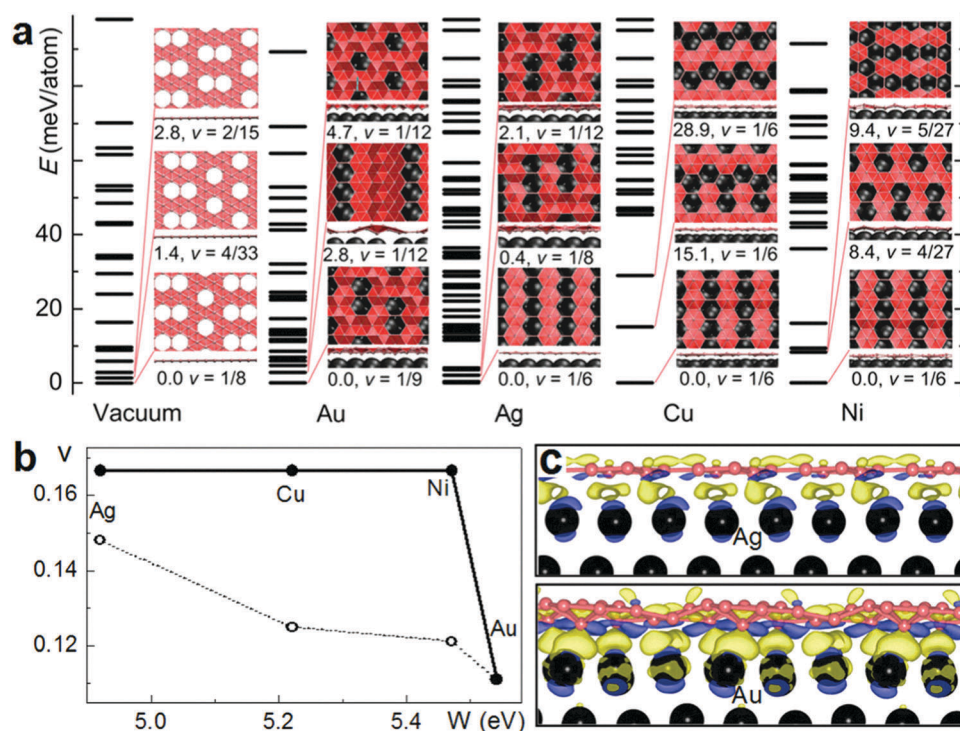


Fig. 5 Structures of 2D boron on metals. (a) Configurational energy spectra of 2D B in a vacuum, on Au, Ag, Cu and Ni. The insets in each column show three most stable structures, and the number below each inset is energy relative to ground states. (b) Vacancy concentration ν of the ground state 2D B as a function of metal work function. The dotted line stands for the results when the boron–metal distance is increased to 5 Å. Iso-surface plots ($0.005 e \text{ \AA}^{-3}$) of charge redistribution between the $\nu_{1/9}$ sheet and Au as well as between the $\nu_{1/6}$ sheet and Cu. Yellow and blue colors represent the electron accumulation and depletion regions, respectively. Boron and metal atoms are colored in pink and black, respectively. Reprinted with permission from ref. 38. Copyright 2015 Wiley.

has been confirmed by subsequent experiments,⁴¹ as discussed in the next section.

3.3 Experimental synthesis of borophenes

Crystalline boron nanostructures. Since the prediction of 2D boron, many experimental attempts have been dedicated to realizing this long-sought material. Early experiments have synthesized boron nanowires,^{99–105} nanoribbons,^{106–109} nanobelts^{110–113} and whiskers,¹⁰⁷ yet all these 1D boron nanostructures either are amorphous or inherit lattice structures from bulk boron. The synthesis methods for fabricating these boron nanostructures comprise non-catalytic and catalytic methods: the former include laser ablation, magnetron sputtering, pyrolysis of diborane, *etc.*, while the latter include CVD using metal alloys as catalysts. It is likely that the absence of 2D sheets from these experiments is due to the lack of a catalytic surface for guiding the boron growth to follow the 2D route. Moreover, the fact that precursors are not pure boron sources may also be detrimental to the nucleation of 2D boron. It is worth mentioning that several research groups have reported growth of single-walled⁸⁸ and multiwalled⁸⁹ boron nanotubes, but the tube walls seem to be crystalline, not layered as in borophenes discussed in this review. Further details on the synthesis, characterization and device applications of 1D boron nanostructures can be found in the dedicated review.¹¹⁴

Very recently, the first 2D boron nanofilms were reported by Tai *et al.* using the conventional CVD method.¹¹⁵ In their experiment,

a mixture of boron and boron oxide powders was heated, to form diboron dioxide vapor at ~ 1400 K, and then deposited onto Cu foils for growth at ~ 1300 K. Nevertheless, the obtained centimeter-wide nanofilms were not the monoatomic layers discussed here but were rather ~ 0.8 nm thick, indicating that the growth of borophenes required a more delicate process.

2D boron monolayers. Following the theory guidelines^{38,39} and perhaps their own intuition, Guisinger and coworkers⁴⁰ have indeed realized monolayer boron sheets on Ag(111) using the molecular beam epitaxy method by direct evaporation of a pure boron source on a clean, single-crystal Ag(111) surface. The boron sheets were characterized to be atomically thin and hundreds of nanometres wide (Fig. 6a and b). Scanning tunneling microscopy (STM) characterization revealed that the monoatomic boron layers not only were really expansive but exhibited different phases depending on the deposition rate. A low deposition rate favors a flat striped phase consisting of a rectangular lattice (Fig. 6c), while increasing the deposition rate increases the coverage of a homogeneous phase appearing as periodically protruded atomic chains (Fig. 6d) in STM images. Moreover, increasing the temperature can transform the flat phase into a new striped phase with periodic nanoscale corrugations. The corrugated stripes are fewer at temperature below 720 K but can reach full coverage as the temperature is increased to ~ 1000 K.

Concurrently, Feng *et al.*⁴¹ performed the synthesis of monolayer boron islands (tens of nanometres wide) on Ag(111) by means of essentially the same method (Fig. 6e). Their results

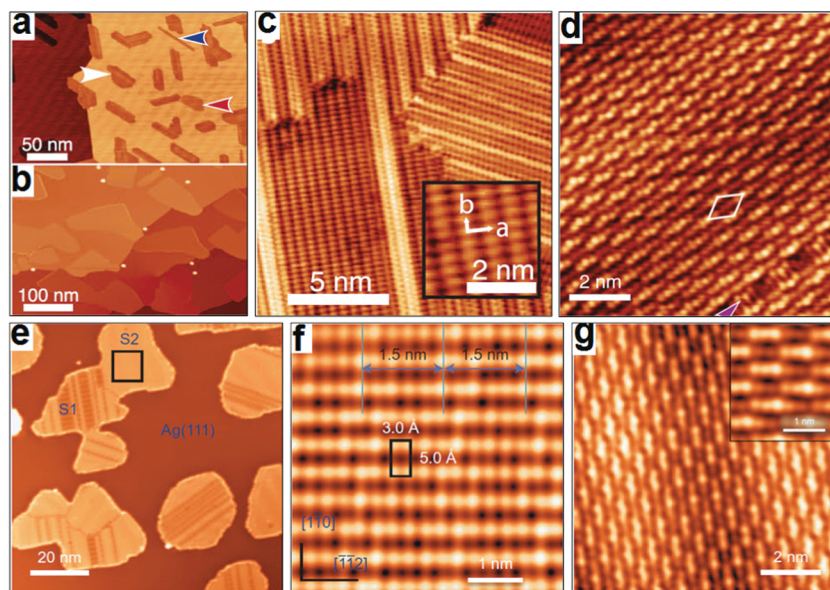


Fig. 6 Experimentally synthesized borophenes on silver. (a and b) Large-scale STM topography images of 2D boron with (a) low ($V_{\text{sample}} = 2.0$ V, $I_t = 100$ pA) and (b) medium coverages ($V_{\text{sample}} = 3.5$ V, $I_t = 100$ pA). Red, white and blue arrows denote regions of homogeneous-phase, striped-phase islands and striped-phase nanoribbons, respectively. (c) STM images of atomic-scale structures for the striped phases ($V_{\text{sample}} = 0.1$ V, $I_t = 1.0$ nA), showing a coexistence of flat and corrugated regions. The inset shows a rectangular lattice with overlaid lattice vectors. (d) STM images for the homogeneous phase ($V_{\text{sample}} = 0.1$ V, $I_t = 1.0$ nA). Reprinted with permission from ref. 40. Copyright 2015 American Association for the Advancement of Science. (e) STM image of 2D boron annealed at 650 K. S1 and S2 indicate two different phases. (f and g) High-resolution STM images of (f) S1 and (g) S2 phases recorded with $V_{\text{sample}} = 1.0$ V. The black rectangle shows the unit cell of the S1 phase, and solid lines denote stripes with 1.5 nm periodicity. The image in g zooms in the region marked by a black square in e and the inset is an image zoomed from g. Reprinted with permission from ref. 41. Copyright 2016 Nature Publishing Group.

also confirm their inherent polymorphism. The samples grown at ~ 570 K show a rectangular lattice with parallel atomic rows in the STM image, referred to as the S1 phase (Fig. 6f), closely resembling the flat striped phase reported by Guisinger *et al.*⁴⁰ When the temperature is increased to 680 K, a new S2 phase consisting of parallel chains was formed (Fig. 6g). The S2 phase can also be transformed from the S1 phase upon annealing the sample to 650 K. This phase exhibits parallel atomic rows as well, yet with alternating brighter and darker segments and a shorter inter-row spacing than that in the S1 phase. The segments are organized in a compact “brick wall” pattern, very similar to the homogeneous phase produced by Guisinger *et al.*⁴⁰ These connections between the two independent experiments underscore the importance of identifying the atomic models for these boron phases.

Atomic models of synthesized 2D boron. Just months prior to the reported experimental realization of borophenes, Zhang *et al.*³⁸ predicted by global minimum search that the $\nu_{1/6}$ sheet, with parallel HH rows spaced by rows of filled hexagons, is the ground state on Ag(111). It was then rather gratifying that the so-called S1 phase in experiment³⁴ was identified to be the very same atomic structure as the $\nu_{1/6}$ sheet (Fig. 7a, top), as supported by simulated STM images (Fig. 7a, bottom) and further corroborated by estimating the density of boron atoms.⁴¹ Such an example case of theory guiding the actual synthesis realized within such a short period of time is rare and very encouraging. It is worth mentioning that the triangular sheet (Fig. 7b, top) was proposed as an atomic model for the flat striped phase in ref. 40, on the basis of a simulated STM image, and apparently it captures the key features of experimental images as well (Fig. 7b, bottom). This discrepancy in model-interpretation is in itself interesting, since the so-called S1 and flat striped phases look very similar in the STM image. The two models have been widely adopted for further exploration of intrinsic

properties and potential applications of borophenes. Based on current experimental characterization, it remains premature to unambiguously affirm which model is the right one. To stimulate further study, we provide two arguments that better support the $\nu_{1/6}$ sheet.

First, *ab initio* calculations show that the $\nu_{1/6}$ sheet is 41 meV per atom more stable than the triangular sheet on Ag(111)¹¹⁶ and matches the lattice constants of Ag(111) (only $\sim 1\%$ mismatch) better than the triangular sheet ($\sim 3.1\%$ off). Second, Zhang *et al.*¹¹⁶ have found that the $\nu_{1/6}$ sheet can energetically accommodate and even favor periodic nanoscale undulations on concertedly reconstructed Ag(111), by virtue of its anisotropic high bending flexibility. Such an undulated $\nu_{1/6}$ sheet can well explain the corrugated phase transformed from the flat striped phase⁴⁰ in terms of topography, wavelength, Moiré pattern, and prevalence of vacancy defects.¹¹⁶ In contrast, the triangular sheet has a finite thickness, which makes the energy cost of corrugation across its ridges prohibitively high,¹¹⁷ unless a structural transition from the triangular to the $\nu_{1/6}$ sheet occurs before the flat-to-corrugated transformation. Such a structural transition lacks evidence in view of the coherent atomic lattice across the interface between the corrugated and flat regions (Fig. 6c). In spite of these arguments, further experimental characterization and theoretical analyses are encouraged to discriminate between the atomic models for these boron phases. Theoretically, an atomistic understanding of growth kinetics and morphology of borophenes will be particularly helpful.

In addition, Feng *et al.*⁴¹ proposed a $\nu_{1/5}$ sheet (labeled χ_3) as an atomic model for the S2 phase (Fig. 7c, top). On Ag, the $\nu_{1/5}$ sheet is nearly as stable as the $\nu_{1/6}$ sheet, with energy difference being within mere 2 meV per atom. Simulated STM images reveal a rhomboidal brick-wall pattern (Fig. 7c, bottom), consistent with experimental images. The stripes with alternate dark and light segments are from the HH rows while the rows

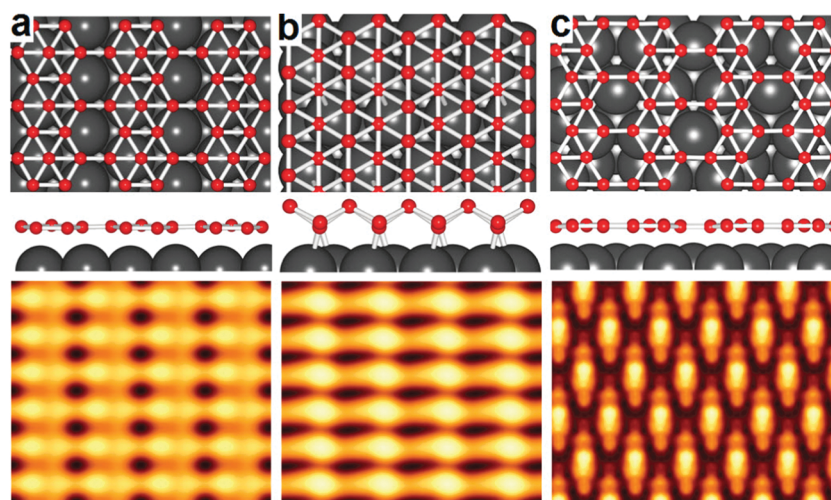


Fig. 7 Structural models of 2D boron on silver. (a) Atomic structure of (top) the $\nu_{1/6}$ sheet and (bottom) simulated STM image, proposed for the flat striped phase in Fig. 6c and the S1 phase in Fig. 6f. (b) Atomic structure of the triangular sheet and simulated STM image, resembling the STM image for the striped phase as well. (c) Atomic structure of the $\nu_{1/5}$ sheet and simulated STM image, proposed for the S2 phase shown in Fig. 6g. V_{sample} is set to 1.0 V for all the STM simulations in constant current mode. The red and black balls denote boron and Ag atoms, respectively. Images were newly simulated and are consistent with those in ref. 40, 41 and 116.

of filled hexagons are located between the stripes (Fig. 7c, bottom), in contrast to the case of the $\nu_{1/6}$ sheet, in which the rows of filled hexagons correspond to the light stripes in the STM image (Fig. 7a, bottom). The $\nu_{1/5}$ model was supported by a subsequent theoretical study⁴⁵ and may also account for the homogeneous phase reported in ref. 40. Another notable fact is that Mannix *et al.* found that lowering the temperature favors the growth of their homogeneous phase, in contrast to observations by Feng *et al.*⁴¹ that the S2 phase is preferred at higher temperature. Mannix *et al.* suggested that the homogeneous phase ($\nu_{1/5}$ sheet) is metastable relative to the striped phase ($\nu_{1/6}$ sheet), whereas Feng *et al.*⁴¹ concluded that the S2 phase ($\nu_{1/5}$ sheet) is more stable than the S1 phase ($\nu_{1/6}$ sheet). This contrast suggests that the growth of borophenes should be determined by an intricate interplay of more factors, such as substrate condition and deposition rate, which calls for an intensive experimental study. Using the same experimental conditions as those in ref. 41, Zhong *et al.* recently reported a new boron phase with hexagonal symmetry on Ag(111), proposed to be the well-known α -sheet.¹¹⁸

3.4 Basic properties of 2D boron

Mechanical properties. Being made up of classical covalent bonds and metallic-like multicenter bonds, borophenes exhibit unique mechanical properties.^{117,119–124} In general, the covalent bonds endow the sheet with considerable strength while the metallic-like multicenter bonds make the structure potentially fluxional. The in-plane stiffness of the synthesized $\nu_{1/6}$ sheet is 218 N m⁻¹ and 205 N m⁻¹ along and across the HH rows,¹²⁵ respectively, both comparable to graphene's 338 N m⁻¹. As long as the 2D boron contains HHs, the in-plane stiffness shows trivial dependence on ν , mainly because the elasticity is dominated by deformation around the HHs.¹¹⁷ Having no HH, the buckled triangular sheet is highly anisotropic, with a stiffness of 398 N m⁻¹ along its ridges^{34,100} and only 163 N m⁻¹ across the ridges. On the other hand, borophenes are flexible during out-of-plane bending. The bending modulus of the $\nu_{1/6}$ sheet is as low as 0.39 eV along the HH rows, about one fourth of graphene's value, and increases to 0.56 eV across the HH rows, showing stronger anisotropy than its in-plane elasticity.¹¹⁷ All other boron sheets with HHs have higher bending moduli but the values remain much smaller than that of graphene. The excellent in-plane stiffness and unusual off-plane flexibility open the possibility of using 2D boron layers as reinforcing elements in advanced composites. Again, the triangular sheet has an exceptionally large bending modulus of 4.9 eV along the ridges due to its off-plane buckling.

Of more interest is the ideal strength of borophenes. It has been shown that the $\nu_{1/6}$ sheet has ideal strengths of 14 N m⁻¹ and 15 N m⁻¹ along and across the HH rows, respectively, close to that of 2D MoS₂¹²⁵ and significantly higher than those of phosphorene^{126,127} and silicene,¹²⁸ yet the critical strains are in the range of 10–15%,^{117,122} much lower than that ($\sim 25\%$) of graphene. Beyond the critical strain, the 2D boron does not undergo structural failure as in the case of other 2D materials, but experiences a structural phase transition. As the tensile

strain increases, B atoms become increasingly easy to re-organize, in a manner that expands the sheet area *via* an increase of HH concentration and thereby relieves the tension. The structural phase transition could toughen the material further, to an extent that it could resist large load even when extremely stretched. Note that the HHs are critically important for the ductile breaking process. Having no HH, the triangular sheet becomes brittle during structural stretching, with the breaking strain estimated to be as low as $\sim 8\%$ when stretched along the ridges.^{100,104}

Electronic properties. While the organizations of chemical bonds in 2D and 3D forms of boron are similar, all 2D boron polymorphs are metallic,^{32,34} in contrast to the insulating nature of their 3D forms. Fig. 8a and b present the band structures¹²⁹ of the $\nu_{1/6}$ and $\nu_{1/5}$ sheets, respectively, calculated using the local density approximation (LDA). The metallic states are mostly derived from the 2p_z state, which is highly delocalized over a large energy window around the Fermi level. In the case of the $\nu_{1/5}$ sheet, the metallicity is also in part contributed by the 2p_x and 2p_y states, which otherwise form a band gap near the Fermi level in the sheets with $\nu = 10\text{--}15\%$.³⁴ The predicted metallicity was confirmed by recent experimental measurements.^{40–42} In particular, Feng *et al.*⁴² performed a detailed analysis of electronic properties of the S1 phase ($\nu_{1/6}$ sheet) on Ag(111) using angle-resolved photoemission spectroscopy (ARPES). Their measurements detected the metallic bands derived from boron (Fig. 8c) and found that its Fermi surface on Ag(111) is composed of one electron pocket (B₁), centered at the *M* point, and a pair of electron pockets (B₂ and B_{2'}), in the vicinity of the *X* point (lower-right panel in Fig. 8c).

A Dirac-cone-like feature can be identified already in the p_z-derived bands of the $\nu_{1/6}$ sheet, appearing at ~ 2 eV above the Fermi level E_F along Γ -*X*, as shown in Fig. 8a. Such band topology can be understood within the simplest single-orbital tight-binding model of this sheet, with just two parameters: the B 2p_z on-site energy, ε_{2p} , and the hopping integral between p_z orbitals on nearest-neighbor B atoms, $t > 0$. Following ref. 130 for instance, the tight-binding Hamiltonian takes the simple form:

$$\hat{H}_{\text{TB}} = -t \begin{pmatrix} \varepsilon_{2p} & h_x & 1 & 0 & h_y \\ h_x^* & \varepsilon_{2p} & h_x^* & 1 & 0 \\ 1 & h_x & \varepsilon_{2p} & h_x & 1 \\ 0 & 1 & h_x^* & \varepsilon_{2p} & h_x^* \\ h_y^* & 0 & 1 & h_x & \varepsilon_{2p} \end{pmatrix}, \quad (2)$$

where $h_x = 1 + \exp(ik_x)$, $h_y = \exp(ik_y)$, and $-\pi \leq k_i \leq \pi$ ($i = x, y$) are the 2D quasi-momentum components. The corresponding band structure is superimposed as black solid lines in Fig. 8a, using $t \approx 1.4$ eV (approximately half of that in graphene¹³¹), and $\varepsilon_{2p} - E_F \approx -1.2$ eV to match the position of the two lowest p_z states of the LDA-calculated bands at the Γ point. Note that even this simple model exhibits two (somewhat “deformed”) conical band crossings in the Brillouin zone (Fig. 9), with Dirac points located at $\pm \frac{2}{3}X$. A more elaborate tight-binding treatment

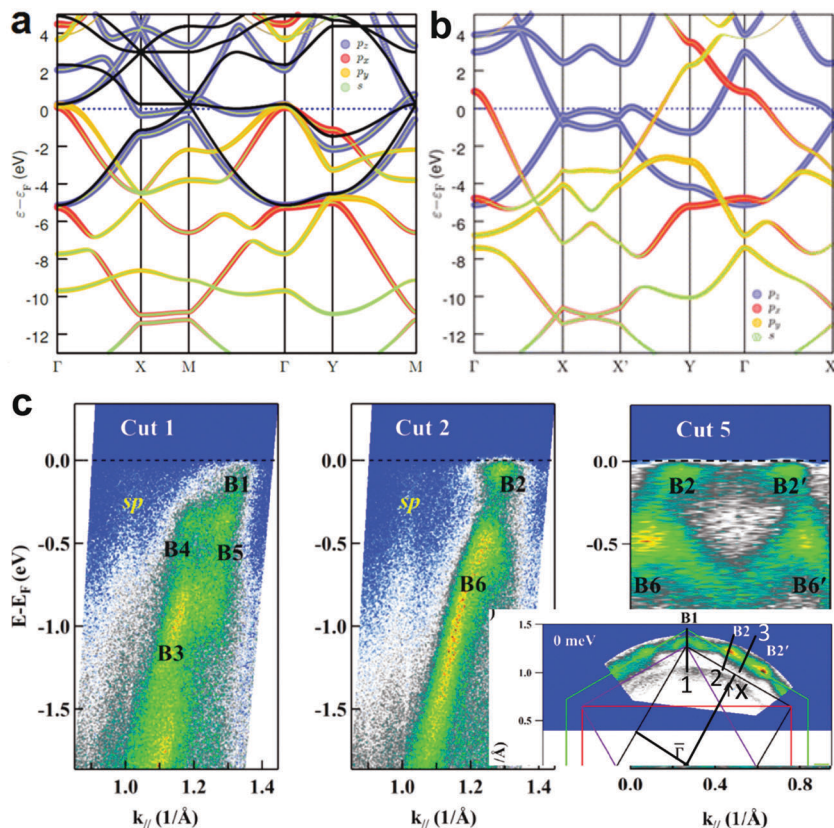


Fig. 8 Electronic properties of 2D boron sheets. (a and b) LDA band structures of (a) the $\nu_{1/6}$ and (b) $\nu_{1/5}$ sheets in a vacuum. Black solid lines in (a) are single-orbital (p_z) tight-binding bands, using $t \approx 1.4$ eV, and $\varepsilon_{2p} - E_F \approx -1.2$ eV. Reprinted with permission from ref. 129. Copyright 2012 American Chemical Society. (c) ARPES intensity plots of the borophene in the S1 phase on silver at $E - E_F = -100$ meV,⁴² taken along different lines in the Brillouin zone, labeled by 1–3 in the inset, where the green lines denote the Brillouin zone of Ag(111). B1–B6 mark the bands of 2D boron and sp marks the bulk sp bands of Ag(111). The intensity plot in the inset is taken at the Fermi surface, i.e. $E - E_F = 0$ meV. Both E_F and ε_F denote the Fermi level. Reprinted with permission from ref. 42. Copyright 2016 American Physical Society.

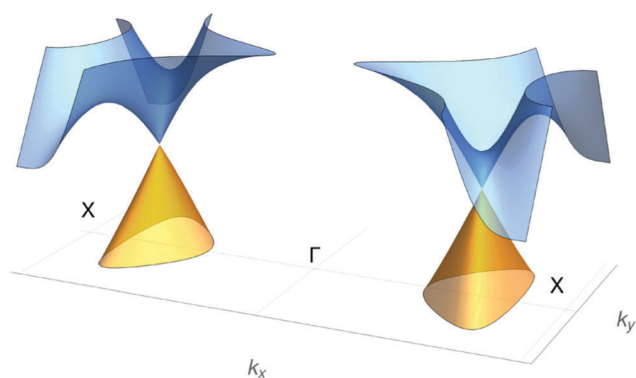


Fig. 9 Dirac cones in the tight-binding bands of the $\nu_{1/6}$ sheet (see also Fig. 8a). Band surfaces are rendered in the energy window $\pm t/2$ relative to the Dirac-point energy, with positive and negative leaves shown in different colors.

is given in ref. 132 and 133. Interestingly, Feng *et al.* indeed observed Dirac cones in the $\nu_{1/6}$ sheet on an Ag(111) substrate in a recent ARPES experiment.¹³³ However, their observed Dirac cones are located ~ 0.25 eV below E_F , in contrast to the level of ~ 2 eV above E_F for the cones shown in Fig. 9. Since theoretical calculations revealed that the Ag substrate can shift E_F of the

$\nu_{1/6}$ sheet upward by only ~ 0.7 eV, the origin of the observed Dirac cones would require a deeper theoretical analysis. It is possible that the $\nu_{1/6}$ sheet possesses more Dirac cones other than those captured in Fig. 9, due to its multiple sublattice sites and a rectangular symmetry. Nevertheless, these ARPES experiments^{36,115} provide solid evidence for another elemental 2D material with massless Dirac fermions, along with graphene and silicene.

The light weight of boron suggests possibly strong electron-phonon coupling, which, along with the intrinsic metallicity, may give rise to conventional, phonon-mediated superconductivity. First-principles calculations¹²⁹ indeed supported intrinsic superconducting behavior, with critical temperature T_c estimated in the range of 10–20 K, depending on the HH concentration. The T_c values are higher than the theoretically computed $T_c \approx 8$ K¹³⁴ and experimentally measured ~ 6 K¹³⁵ for Li-decorated graphene. Possible superconductivity is also suggested for thicker boron films.¹³⁶ This result renders 2D boron an attractive testbed for exploring the true 2D limit of conventional superconductivity. It is worth noting that accurate DFT calculations¹²⁹ reveal characteristic phonon instabilities in the free-standing polymorphs. On a suitable metal substrate, such supported polymorphs would be naturally stabilized, but stronger adhesion,

for instance, may eventually reduce T_c . Such suppression of T_c seems to be suggested in subsequent calculations for the triangular B sheet (Fig. 3c, left) on Ag(111).¹³⁷ It is plausible, however, that 2D boron is stabilized by an inert protecting layer such as 2D hexagonal h-BN, in which case the superconducting behavior may well be preserved.

Furthermore, borophenes can be used to possibly build thick 2D boron structures with novel electronic properties. Global minimum search based on evolutionary algorithms identified a boron nanofilm with $Pmmn$ symmetry, which has a distorted Dirac cone near the Fermi level.³⁶ Later on, a 2D ionic boron, composed of a layer of vertically arranged B_2 dimers sandwiched by two graphene-like boron planes, was reported to have double Dirac cones.¹³⁸ All these boron nanofilms have a honeycomb lattice as the skeleton and the remaining boron atoms as donors, which make the honeycomb skeleton isoelectronic to graphene, thereby creating the Dirac-like electronic states. In hindsight, this justifies and explains the success of the first cluster-expansion study,³⁴ which essentially assumed a 'configurationally inactive' boron honeycomb sublattice in the attempt to explore configurational diversity of 2D boron polymorphs. Using an evolutionary approach, He *et al.* reported a boron nanofilm on Pb(110) with a graphene-like structure, comprising three inter-bonded atomic layers, which has peculiar double Dirac cones.¹³⁹ Recently, a boron nanofilm composed of B_{20} clusters arranged in a hexagonal network was predicted to have antiferromagnetic ordering.¹⁴⁰ Structurally being closer to bulk boron, these thicker boron nanofilms are lower in energy than monolayer borophenes, but their existence still lacks experimental support.

Chemical properties. The boron sheets were demonstrated to be quite inert to oxidation,⁴¹ which should be ascribed to their high planarity that may stabilize electronic states in a similar way to electronic conjugation in graphene. A certain content of oxygen was detected in borophene samples upon exposing to air under ambient conditions, but the oxidation was found to occur mostly at the edges of boron islands, which are chemically reactive due to active edge states. Instead, the regions with perfect lattice remain almost intact, even when the samples are exposed to high doses of oxygen. Nevertheless, the borophenes cannot compete with other popular 2D materials (*e.g.*, graphene) in terms of chemical stability and can be readily contaminated upon long-time exposure to air, as demonstrated by Guisinger *et al.*⁴⁰ This is in line with the previous prediction that boron sheets on metals are reactive enough to serve as a catalyst for the hydrogen evolution reaction.³⁸ Such a chemical property has never been possessed by other 2D materials (at least until the recent discovery of catalytically surface-active metal dichalcogenides¹⁴¹) and could be harnessed for achieving a rich spectrum of functionalities through functionalization with various chemical species, such as hydrogen that could result in 2D boron hydrides with Dirac fermions.^{120,142–144} Meanwhile, it also highlights the need for developing packing techniques for fabricating air-stable borophene-based devices. For example, the boron sheets could be sealed from air by depositing a capping layer. Guisinger *et al.*⁴⁰ have demonstrated that the

oxidation of borophenes can be greatly impeded by a silicon/silicon oxide capping layer.

The 2D boron is predicted to have a high capability of accommodating point defects. For a flat $\nu_{1/6}$ sheet on Ag(111), the formation energy is estimated to be in the range of 1.8–3 eV for a monovacancy and 2.4–4.2 eV for a divacancy,¹¹⁶ depending on the defect site in the lattice, much lower than ~ 7.5 eV^{145,146} for a monovacancy in graphene. The low formation energies of vacancies are attributed to the unusual atomic reconstruction near the defect that efficiently passivates the dangling bonds thereof. The defect-induced reconstruction is facilitated by the delocalized multicenter bonds and thus offers greater energy relief than those in other strongly covalent 2D materials.

4. Challenges to move forward

While borophenes have been synthesized, moving this new material into physical experimentation or even practical applications is hampered by a number of issues. The urgent issues would be the transfer of borophenes from Ag(111) as well as the controlled synthesis of large-scale, high-quality samples. In this section, we analyze these challenges and discuss possible directions to align future works.

4.1 Transfer of 2D boron

Prior to transfer, it is important to know how strongly borophene adheres to the Ag surface. Earlier estimates³⁹ indicated weak adhesion on the (111) surfaces of Ag and Au. The adhesion energy between the $\nu_{1/6}$ sheet and Ag(111) is $\gamma = 0.04$ eV \AA^{-2} ,¹¹⁶ only twice that (0.02 eV \AA^{-2}) for graphene to Cu(111).¹⁴⁷ However, the chemical reactivity of 2D boron precludes the use of common transfer methods adopted for graphene, especially those involving solutions. Actually, silicene has a much stronger adhesion on Ag than borophenes, but even silicene has been sufficiently cleanly transferred from Ag(111) substrates *via* an encapsulated delamination method.¹⁴⁸ Compared to silicene, borophenes have higher in-plane stiffness and excellent flexibility against bending.¹¹⁷ These facts lead one to propose a transfer method by peeling borophenes off the substrate, in a manner similar to mechanical exfoliation of graphene. The transfer process is schematically illustrated in Fig. 10, including the following key steps: (i) attaching a metal pad at one end of the boron domain, (ii) lifting the pad to progressively peel the 2D boron off the silver, (iii) transferring the detached boron layer onto a target substrate and (iv) removal of the pad. To make sure that the boron layer will not fall off the pad during the transfer, the pad must adhere with boron more strongly than Ag and should be as wide as the boron domain in the direction perpendicular to the movement; in principle, the mechanical configuration can be optimized quantitatively, to reduce experimental trial-error expense. Previous DFT calculations³⁸ indicated that Cu and Ni can serve as the pad. The threshold force for lifting can be estimated as $f = w\gamma = 0.04w$ eV \AA^{-1} , where w is the width of boron islands. This method appears promising for separating

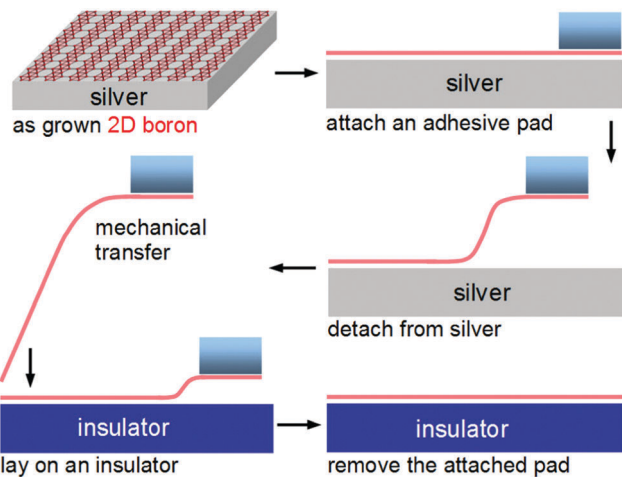


Fig. 10 Schematic illustration of separating borophenes from silver. Key steps: adhesive pad attached, lift from Ag, mechanical transfer of boron onto a target substrate and pad removal.

borophenes once the process can be carefully controlled, even though further improvement may be warranted.

4.2 Large-scale synthesis of 2D boron

Controlled synthesis of large-scale, quality samples is another prerequisite for realizing any prospective industrial applications of 2D boron. Toward this end, the CVD method remains as the first choice. However, years of attempts using this method resulted in amorphous structures,^{103,149,150} clumps, or thick films.¹¹⁵ By closely examining their growth conditions and precursors, we provide several recipes that may help the CVD synthesis of borophenes.

The growth temperature is the first critical factor. High temperature may activate the nucleation along the 3D route and yield boron films, whereas low temperature cannot overcome the barrier required for 2D growth and results in amorphous clusters.⁴¹ Thus, the growth temperature needs to be carefully controlled, to an extent that it is enough to activate the 2D nucleation but not for 3D nucleation. Second, the precursors should be purified boron. Other elements mixed in the precursors, such as hydrogen and oxygen, may stabilize the 3D-nucleus by passivating dangling bonds on its surfaces and thereby suppress the corresponding nucleation barrier. According to ref. 115, the presence of oxygen in the precursors might be one of the reasons for the yield of boron nanofilms. Third, an atomically flat metal substrate is ideal for producing large-scale boron islands. Rough substrates could favor the nucleation of 3D clusters due to local increase of interaction area, thus not conducive to 2D growth. Other factors, such as deposition rate and vapor pressure, should also be carefully tested.

5. Perspective

5.1 Hybrids with other 2D materials

Electronic devices often require the integration of different materials with electronically distinct properties. The application of borophenes in nanodevices will be greatly promoted by

the fabrication of hybridized atomic layers composed of borophenes and other 2D materials. Electronically, borophenes are the first metallic 2D material made of a light element, in contrast to other 2D materials that often have a band gap. Interfacing boron sheets with other semiconducting 2D materials could generate, e.g., 2D metal–semiconductor co-planar junctions.¹⁵¹ It will be useful to see what 2D materials can form an ohmic contact with borophenes and what materials result in what degree of Schottky barrier. The in-plane heterostructures with an ohmic contact would allow the integration of semiconducting channels and electrodes within one material, while those with a Schottky barrier can be used to design atomically thin diodes and transistors. Very recently, Liu and coworkers¹⁵² demonstrated spontaneous formation of borophene/organic lateral heterostructures by depositing perylene-3,4,9,10-tetracarboxylic dianhydrides onto submonolayer borophene on Ag(111) substrates. The heterostructures were connected by weak chemical interaction between the borophene and organic molecules, with the interface revealed to be electronically abrupt.¹³¹ On the other hand, sandwiching the borophenes between insulating h-BN layers will allow an electrically conductive atomic layer encapsulated by chemically inert, thermally stable, atomically smooth skins. Such a system is expected to well preserve the intrinsic properties of borophenes, ideal for fabricating high performance borophene-based devices.

5.2 Other possible novel properties

Since borophenes are strongly metallic, they should exhibit intrinsic plasmons confined in 2D space to allow novel manipulation of light. In particular, the 2D boron can carry a high conductive electron density, σ , independent of the Fermi level, opening a possibility to extend the plasmon energy (frequency $\omega_{\text{pl}} \propto \sqrt{\sigma}$) into the near-visible range, in contrast to graphene where plasmons, despite being controllable by gating, are usually at mid-infrared and longer wavelength.^{153,154} The light–metal interaction in 2D boron may be further enhanced by combining with conventional plasmonics, such as noble metals. In addition, the intrinsically metallic 2D boron will accommodate the 2D electron gas that could give rise to a quantum Hall effect under strong perpendicular magnetic fields. Yet, observing the quantum Hall effect should be facility-demanding, because electronic mobility in such type of 2D metal is relatively low, so that the energy distances between Landau levels are too small to easily discern in experiments.

5.3 Potential applications

The lightweight and excellent mechanical properties of 2D boron can be harnessed in designing advanced composites. For one thing, the 2D boron can resist a large load, comparable to graphene, before failure. For another, the reactivity of 2D boron facilitates covalent bonding to the host-matrix that enables efficient load transfer. Experimental effort along this direction is highly encouraged. The abundance of structural information on 2D boron also prompted studies of their electronic transport properties.^{155,156} Boron nanotubes, especially those rolled up from the α sheet, are predicted to be electrically more conductive¹⁵⁵ than carbon nanotubes. These results suggest the possibility of using boron nanotubes as

interconnects and contacts in future nanoscale devices, which circumvents the issue of chirality dependence of electrical conductivity in carbon nanotubes. Recent synthesis of ~ 10 nm narrow borophene nanoribbons on Ag(110) substrates opens another dimension of controlling electronics of such interconnects by their width.¹⁵⁷ In theory, ultimately thin ribbons would be more stable as a 2-atom-wide metallic ribbon than as a single-atom chain, while stretching should switch it to a chain-like semiconductor.^{158,159} In addition, the excellent structural flexibility makes metallic borophenes promising for potential applications in the emerging flexible electronics.

Borophenes also appear to be attractive materials for energy storage. Their capacities of hydrogen storage have been compared to those of graphene.¹⁶⁰ The binding of molecular hydrogen to the boron sheet is stronger than that to graphene, due to its more reactive basal plane. It has also been found that dispersion of alkali metal (Li, Na, and K) atoms onto the boron sheet markedly increases hydrogen binding energies and storage capacities. Meanwhile, the 2D boron provides a template for creating a stable lattice of strongly bound metal atoms with a large nearest neighbor distance. When coated with Ca and Sc, α -boron sheets are found to be excellent adsorbents for ambient CO₂ capture with remarkably high adsorption energies of up to 3.0 eV.¹⁶¹ Other theoretical studies also revealed boron sheets as a promising electrode material with high electrochemical performance for both Li-ion and Na-ion batteries.^{162–165} However, all these works missed to notice that borophenes may undergo structural phase transition upon adsorption of metal atoms as a result of electronic donation from the adsorbates, which requires further examination.

Since boron can combine with most of other elements, it has been used for designing new compound 2D materials. At present, theoretical works have explored the stability of 2D Si_xB_{1-x},¹⁶⁶ C_xB_{1-x},^{167,168} and BP¹⁶⁹ monolayers. The 2D silicon borides and boron carbides are all metallic, regardless of the stoichiometry, whereas the 2D boron phosphides are polymorphic and can be metallic or semiconducting depending on whether the boron atoms are dimerized or not. In addition, the 2D boron has been used as the basis in the efforts for uncovering new 2D metal borides through combining with various metals. BeB₂,¹⁷⁰ TiB₂,¹⁷¹ BeB₂,¹⁷² FeB₆,¹⁷³ and FeB₂¹⁷⁴ monolayers have been demonstrated to possess satisfactorily high stability and intriguing properties. In particular, the TiB₂, BeB₂, and FeB₂ sheets possess Dirac-like electronic dispersion near the Fermi level. Note that the Dirac states in the TiB₂ and FeB₂ sheets primarily originate from metal atoms forming a triangular network and bear lesser contribution from the layer of honeycomb boron lattices. Furthermore, two-dimensional Dirac materials can be designed by insertion of chemical elements into borophene, as β_{12} -XB₅ (X = H, F, Cl).¹⁷⁵

6. Conclusions and outlook

Despite being the fifth element, boron offers more puzzles in its structural organization than its neighbors in the periodic table.

It displays multiple bulk phases, and its nanostructures are even more diverse, ranging from planar and cage-like clusters, 1D nanotubes and nanowires to 2D sheets and nanofilms. In particular, the 2D boron is of special interest as a potentially new material and as a conceptual precursor for boron nanostructures of other dimensionalities. Moreover, the metallic character of 2D boron makes it complementary to graphene, h-BN, and transition metal dichalcogenides that are bound to serve as ultimate building components in future devices. However, borophenes exhibit inherent polymorphism and are less stable than all bulk phases, imposing a challenge for their synthesis. Here, we have reviewed current theoretical progress in proposing atomic structures, predicting physical properties and exploring potential applications of 2D boron as well as experimental discoveries and further advances in synthesizing this long-sought material. We particularly focused on elucidating the pioneering role of theory in the creation of 2D boron: from understanding the structures and bonding, to offering practical routes for synthesis, to accurately identifying the atomic structure that 2D boron should have on several technologically important substrates. Benefiting from theoretical suggestions, recent experiments have successfully realized borophenes on silver using the molecular beam epitaxy method, which not only confirmed their structural polymorphism and metallicity but also uncovered the same atomic model on the same substrate as theory predicted earlier. One can already argue that these developments from a theoretical concept, to search and to realization, offer a showcase-example of materials genome initiative (MGI) whose mission is to discover and deploy advanced materials twice faster, at a fraction of the cost.¹⁷⁶ However, many issues remain on the way to using this material, calling for continuous joint efforts from both theorists and experimentalists. First, more intensive theoretical works are anticipated to discover new models of 2D boron in different environments, reveal how the material is grown from an atomistic point of view, and explore novel properties for extending applications. Second, experimental attempts should be dedicated to developing efficient transfer methods for lifting borophenes off substrates and more practical CVD methods that allow controlled growth of large-scale samples. To motivate interest and in an attempt to guide further research, we have discussed possible routes towards addressing these issues experimentally. Finally, based on the properties borophenes have shown, we also discussed their potential applications, such as designing 2D heterostructures, advanced composites and energy storage materials as well as fabricating flexible electronics.

Conflicts of interest

There are no conflicts to declare.

Acknowledgements

We gratefully acknowledge support by the Department of Energy BES grant DE-SC0012547, and by the Office of Naval Research grant N00014-15-1-2372. Z. Z. also acknowledges the support of NSFC (11772153).

Notes and references

- 1 A. J. Mannix, B. Kiraly, M. C. Hersam and N. P. Guisinger, *Nat. Rev. Chem.*, 2017, **1**, 0014.
- 2 A. R. Oganov and V. Solozhenko, *J. Superhard Mater.*, 2009, **31**, 285–291.
- 3 L. Bolaños, K. Lukaszewski, I. Bonilla and D. Blevins, *Plant Physiol. Biochem.*, 2004, **42**, 907–912.
- 4 A. R. Pitochelli and M. F. Hawthorne, *J. Am. Chem. Soc.*, 1960, **82**, 3228–3229.
- 5 M. F. Hawthorne, D. C. Young and P. A. Wegner, *J. Am. Chem. Soc.*, 1965, **87**, 1818–1819.
- 6 J. L. Gay-Lussac and L. J. Thénard, *Ann. Chim. Phys.*, 1808, **68**, 169–174.
- 7 H. Davy, *Philos. Trans. R. Soc. London*, 1808, **98**, 333–370.
- 8 D. E. Sands and J. Hoard, *J. Am. Chem. Soc.*, 1957, **79**, 5582–5583.
- 9 P. Ball, *Nat. Mater.*, 2010, **9**, 6.
- 10 A. R. Oganov, J. Chen, C. Gatti, Y. Ma, Y. Ma, C. W. Glass, Z. Liu, T. Yu, O. O. Kurakevych and V. L. Solozhenko, *Nature*, 2009, **460**, 292.
- 11 H. F. Schaefer III and F. E. Harris, *Phys. Rev.*, 1968, **167**, 67.
- 12 B. Albert and H. Hillebrecht, *Angew. Chem., Int. Ed.*, 2009, **48**, 8640–8668.
- 13 A. N. Alexandrova, A. I. Boldyrev, H.-J. Zhai and L.-S. Wang, *Coord. Chem. Rev.*, 2006, **250**, 2811–2866.
- 14 A. P. Sergeeva, I. A. Popov, Z. A. Piazza, W.-L. Li, C. Romanescu, L.-S. Wang and A. I. Boldyrev, *Acc. Chem. Res.*, 2014, **47**, 1349–1358.
- 15 L.-S. Wang, *Int. Rev. Phys. Chem.*, 2016, **35**, 69–142.
- 16 W. Huang, A. P. Sergeeva, H.-J. Zhai, B. B. Averkiev, L.-S. Wang and A. I. Boldyrev, *Nat. Chem.*, 2010, **2**, 202–206.
- 17 Z. A. Piazza, H.-S. Hu, W.-L. Li, Y.-F. Zhao, J. Li and L.-S. Wang, *Nat. Commun.*, 2014, **5**, 3113.
- 18 A. P. Sergeeva, D. Y. Zubarev, H.-J. Zhai, A. I. Boldyrev and L.-S. Wang, *J. Am. Chem. Soc.*, 2008, **130**, 7244–7246.
- 19 W. L. Li, Y. F. Zhao, H. S. Hu, J. Li and L. S. Wang, *Angew. Chem., Int. Ed.*, 2014, **53**, 5540–5545.
- 20 H.-R. Li, T. Jian, W.-L. Li, C.-Q. Miao, Y.-J. Wang, Q. Chen, X.-M. Luo, K. Wang, H.-J. Zhai and S.-D. Li, *Phys. Chem. Chem. Phys.*, 2016, **18**, 29147–29155.
- 21 H.-J. Zhai, Y.-F. Zhao, W.-L. Li, Q. Chen, H. Bai, H.-S. Hu, Z. A. Piazza, W.-J. Tian, H.-G. Lu and Y.-B. Wu, *Nat. Chem.*, 2014, **6**, 727–731.
- 22 N. G. Szwacki, A. Sadrzadeh and B. I. Yakobson, *Phys. Rev. Lett.*, 2007, **98**, 166804.
- 23 N. G. Szwacki, A. Sadrzadeh and B. I. Yakobson, *Phys. Rev. Lett.*, 2008, **100**, 159901.
- 24 G. Gopakumar, M. T. Nguyen and A. Ceulemans, *Chem. Phys. Lett.*, 2008, **450**, 175–177.
- 25 H. Li, N. Shao, B. Shang, L.-F. Yuan, J. Yang and X. C. Zeng, *Chem. Commun.*, 2010, **46**, 3878–3880.
- 26 J. Zhao, L. Wang, F. Li and Z. Chen, *J. Phys. Chem. A*, 2010, **114**, 9969–9972.
- 27 D. L. Prasad and E. D. Jemmis, *Phys. Rev. Lett.*, 2008, **100**, 165504.
- 28 S. De, A. Willand, M. Amsler, P. Pochet, L. Genovese and S. Goedecker, *Phys. Rev. Lett.*, 2011, **106**, 225502.
- 29 X.-Q. Wang, *Phys. Rev. B: Condens. Matter Mater. Phys.*, 2010, **82**, 153409.
- 30 F. Li, P. Jin, D.-E. Jiang, L. Wang, S. B. Zhang, J. Zhao and Z. Chen, *J. Chem. Phys.*, 2012, **136**, 074302.
- 31 E. S. Penev, V. I. Artyukhov, F. Ding and B. I. Yakobson, *Adv. Mater.*, 2012, **24**, 4956–4976.
- 32 H. Tang and S. Ismail-Beigi, *Phys. Rev. Lett.*, 2007, **99**, 115501.
- 33 X. Yang, Y. Ding and J. Ni, *Phys. Rev. B: Condens. Matter Mater. Phys.*, 2008, **77**, 041402.
- 34 E. S. Penev, S. Bhowmick, A. Sadrzadeh and B. I. Yakobson, *Nano Lett.*, 2012, **12**, 2441–2445.
- 35 Y. Wang, J. Lv, L. Zhu and Y. Ma, *Phys. Rev. B: Condens. Matter Mater. Phys.*, 2010, **82**, 094116.
- 36 X.-F. Zhou, X. Dong, A. R. Oganov, Q. Zhu, Y. Tian and H.-T. Wang, *Phys. Rev. Lett.*, 2014, **112**, 085502.
- 37 Z. Zhang, X. Liu, J. Yu, Y. Hang, Y. Li, Y. Guo, Y. Xu, X. Sun, J. Zhou and W. Guo, *Wiley Interdiscip. Rev.: Comput. Mol. Sci.*, 2016, **6**, 324–350.
- 38 Z. Zhang, Y. Yang, G. Gao and B. I. Yakobson, *Angew. Chem., Int. Ed.*, 2015, **54**, 13022–13026.
- 39 Y. Liu, E. S. Penev and B. I. Yakobson, *Angew. Chem., Int. Ed.*, 2013, **52**, 3156–3159.
- 40 A. J. Mannix, X.-F. Zhou, B. Kiraly, J. D. Wood, D. Alducin, B. D. Myers, X. Liu, B. L. Fisher, U. Santiago, J. R. Guest, M. J. Yacaman, A. Ponce, A. R. Oganov, M. C. Hersam and N. P. Guisinger, *Science*, 2015, **350**, 1513–1516.
- 41 B. Feng, J. Zhang, Q. Zhong, W. Li, S. Li, H. Li, P. Cheng, S. Meng, L. Chen and K. Wu, *Nat. Chem.*, 2016, **8**, 563–568.
- 42 B. Feng, J. Zhang, R.-Y. Liu, T. Iimori, C. Lian, H. Li, L. Chen, K. Wu, S. Meng, F. Komori and I. Matsuda, *Phys. Rev. B: Condens. Matter Mater. Phys.*, 2016, **94**, 041408.
- 43 Z. Zhang, E. S. Penev and B. I. Yakobson, *Nat. Chem.*, 2016, **8**, 525–527.
- 44 S. Xu, Y. Zhao, J. Liao, X. Yang and H. Xu, *Nano Res.*, 2016, **9**, 2616–2622.
- 45 H. Shu, F. Li, P. Liang and X. Chen, *Nanoscale*, 2016, **8**, 16284–16291.
- 46 A. N. Alexandrova and A. I. Boldyrev, *J. Chem. Theory Comput.*, 2005, **1**, 566–580.
- 47 A. P. Sergeeva, B. B. Averkiev, H.-J. Zhai, A. I. Boldyrev and L.-S. Wang, *J. Chem. Phys.*, 2011, **134**, 224304.
- 48 D. J. Wales and J. P. Doye, *J. Phys. Chem. A*, 1997, **101**, 5111–5116.
- 49 Z. A. Piazza, W.-L. Li, C. Romanescu, A. P. Sergeeva, L.-S. Wang and A. I. Boldyrev, *J. Chem. Phys.*, 2012, **136**, 104310.
- 50 J. H. Holland, *Adaptation in natural and artificial systems: an introductory analysis with applications to biology, control, and artificial intelligence*, MIT Press, 1992.
- 51 S. Woodley, P. Battle, J. Gale and C. A. Catlow, *Phys. Chem. Chem. Phys.*, 1999, **1**, 2535–2542.
- 52 A. R. Oganov and C. W. Glass, *J. Chem. Phys.*, 2006, **124**, 244704.
- 53 S. Curtarolo, D. Morgan, K. Persson, J. Rodgers and G. Ceder, *Phys. Rev. Lett.*, 2003, **91**, 135503.

- 54 D. W. Hofmann and J. Apostolakis, *J. Mol. Struct.*, 2003, **647**, 17–39.
- 55 A. N. Alexandrova, A. I. Boldyrev, H.-J. Zhai and L.-S. Wang, *J. Phys. Chem. A*, 2004, **108**, 3509–3517.
- 56 H.-J. Zhai, B. Kiran, J. Li and W. Lai-Sheng, *Nat. Mater.*, 2003, **2**, 827.
- 57 B. Kiran, S. Bulusu, H.-J. Zhai, S. Yoo, X. C. Zeng and L.-S. Wang, *Proc. Natl. Acad. Sci. U. S. A.*, 2005, **102**, 961–964.
- 58 Y.-J. Wang, Y.-F. Zhao, W.-L. Li, T. Jian, Q. Chen, X.-R. You, T. Ou, X.-Y. Zhao, H.-J. Zhai and S.-D. Li, *J. Chem. Phys.*, 2016, **144**, 064307.
- 59 J. Zhao, X. Huang, R. Shi, H. Liu, Y. Su and R. B. King, *Nanoscale*, 2015, **7**, 15086–15090.
- 60 Y. Yang, Z. Zhang, E. S. Penev and B. I. Yakobson, *Nanoscale*, 2017, **9**, 1805–1810.
- 61 Y. Mu, Q. Chen, N. Chen, H.-G. Lu and S.-D. Li, *Phys. Chem. Chem. Phys.*, 2017, **19**, 19890–19895.
- 62 C. Li, J. Liu, S. Zhang, G. Lefkidis and W. Hübner, *Carbon*, 2015, **87**, 153–162.
- 63 C. Li, J. Liu, G. Lefkidis and W. Hübner, *Phys. Chem. Chem. Phys.*, 2017, **19**, 673–680.
- 64 H.-R. Li, H. Liu, X. Tian, W.-Y. Zan, Y. Mu, H.-G. Lu, J. Li, Y. Wang and S.-D. Li, *Phys. Chem. Chem. Phys.*, 2017, **19**, 27025–27030.
- 65 Z. Zhang, S. N. Shirodkar, Y. Yang and B. I. Yakobson, *Angew. Chem., Int. Ed.*, 2017, DOI: 10.1002/anie.201705459.
- 66 W.-L. Li, R. Pal, Z. A. Piazza, X. C. Zeng and L.-S. Wang, *J. Chem. Phys.*, 2015, **142**, 204305.
- 67 L. S. Wang, H. S. Cheng and J. Fan, *J. Chem. Phys.*, 1995, **102**, 9480–9493.
- 68 K. Novoselov, A. Geim, S. Morozov, D. Jiang, M. Katsnelson, I. Grigorieva, S. Dubonos and A. Firsov, *Nature*, 2005, **438**, 197.
- 69 Z. Zhang and W. Guo, *Phys. Rev. B: Condens. Matter Mater. Phys.*, 2008, **77**, 075403.
- 70 J. Yin, J. Li, Y. Hang, J. Yu, G. Tai, X. Li, Z. Zhang and W. Guo, *Small*, 2016, **12**, 2942–2968.
- 71 Z. Zhang, X. Zou, V. H. Crespi and B. I. Yakobson, *ACS Nano*, 2013, **7**, 10475–10481.
- 72 M. Chhowalla, H. S. Shin, G. Eda, L.-J. Li, K. P. Loh and H. Zhang, *Nat. Chem.*, 2013, **5**, 263.
- 73 L. Li, Y. Yu, G. J. Ye, Q. Ge, X. Ou, H. Wu, D. Feng, X. H. Chen and Y. Zhang, *Nat. Nanotechnol.*, 2014, **9**, 372–377.
- 74 P. Vogt, P. De Padova, C. Quaresima, J. Avila, E. Frantzeskakis, M. C. Asensio, A. Resta, B. Ealet and G. Le Lay, *Phys. Rev. Lett.*, 2012, **108**, 155501.
- 75 B. Feng, Z. Ding, S. Meng, Y. Yao, X. He, P. Cheng, L. Chen and K. Wu, *Nano Lett.*, 2012, **12**, 3507–3511.
- 76 Y. Xu, B. Yan, H.-J. Zhang, J. Wang, G. Xu, P. Tang, W. Duan and S.-C. Zhang, *Phys. Rev. Lett.*, 2013, **111**, 136804.
- 77 F. Zhu, W. Chen, Y. Xu, C. Gao, D. Guan, C. Liu, D. Qian, S. Zhang and J. Jia, *Nat. Mater.*, 2015, **14**, 1020.
- 78 S. Suehara, T. Aizawa and T. Sasaki, *Phys. Rev. B: Condens. Matter Mater. Phys.*, 2010, **81**, 085423.
- 79 N. Qin, S.-Y. Liu, Z. Li, H. Zhao and S. Wang, *J. Phys.: Condens. Matter*, 2011, **23**, 225501.
- 80 I. Boustani, A. Quandt, E. Hernández and A. Rubio, *J. Chem. Phys.*, 1999, **110**, 3176–3185.
- 81 M. H. Evans, J. Joannopoulos and S. T. Pantelides, *Phys. Rev. B: Condens. Matter Mater. Phys.*, 2005, **72**, 045434.
- 82 S. Chacko, D. Kanhere and I. Boustani, *Phys. Rev. B: Condens. Matter Mater. Phys.*, 2003, **68**, 035414.
- 83 I. Boustani, A. Rubio and J. A. Alonso, *Chem. Phys. Lett.*, 1999, **311**, 21–28.
- 84 I. Boustani, *Phys. Rev. B: Condens. Matter Mater. Phys.*, 1997, **55**, 16426.
- 85 K. C. Lau and R. Pandey, *J. Phys. Chem. C*, 2007, **111**, 2906–2912.
- 86 J. Kunstmann and A. Quandt, *Phys. Rev. B: Condens. Matter Mater. Phys.*, 2006, **74**, 035413.
- 87 I. Cabria, M. López and J. Alonso, *Nanotechnology*, 2006, **17**, 778.
- 88 D. Ciuparu, R. F. Klie, Y. Zhu and L. Pfefferle, *J. Phys. Chem. B*, 2004, **108**, 3967–3969.
- 89 F. Liu, C. Shen, Z. Su, X. Ding, S. Deng, J. Chen, N. Xu and H. Gao, *J. Mater. Chem.*, 2010, **20**, 2197–2205.
- 90 H. Tang and S. Ismail-Beigi, *Phys. Rev. B: Condens. Matter Mater. Phys.*, 2010, **82**, 115412.
- 91 J. M. Sanchez, F. Ducastelle and D. Gratias, *Phys. A*, 1984, **128**, 334–350.
- 92 X. Wu, J. Dai, Y. Zhao, Z. Zhuo, J. Yang and X. C. Zeng, *ACS Nano*, 2012, **6**, 7443–7453.
- 93 X. Yu, L. Li, X.-W. Xu and C.-C. Tang, *J. Phys. Chem. C*, 2012, **116**, 20075–20079.
- 94 H. Lu, Y. Mu, H. Bai, Q. Chen and S.-D. Li, *J. Chem. Phys.*, 2013, **138**, 024701.
- 95 N. Karmodak and E. D. Jemmis, *Angew. Chem., Int. Ed.*, 2017, **56**, 10093–10097.
- 96 H. Tang and S. Ismail-Beigi, *Phys. Rev. B: Condens. Matter Mater. Phys.*, 2009, **80**, 134113.
- 97 H. Liu, J. Gao and J. Zhao, *Sci. Rep.*, 2013, **3**, 3238.
- 98 Y. Zhao, C. Ban, Q. Xu, S.-H. Wei and A. C. Dillon, *Phys. Rev. B: Condens. Matter Mater. Phys.*, 2011, **83**, 035406.
- 99 J. Wu, S. Yun, A. Dibos, D.-K. Kim and M. Tidrow, *Microelectron. J.*, 2003, **34**, 463–470.
- 100 X. Meng, J. Hu, Y. Jiang, C. Lee and S. Lee, *Chem. Phys. Lett.*, 2003, **370**, 825–828.
- 101 L. Cao, Z. Zhang, L. Sun, C. Gao, M. He, Y. Wang, Y. Li, X. Zhang, G. Li, J. Zhang and W. K. Wang, *Adv. Mater.*, 2001, **13**, 1701–1704.
- 102 L. Cao, K. Hahn, Y. Wang, C. Scheu, Z. Zhang, C. Gao, Y. Li, X. Zhang, L. Sun and W. Wang, *Adv. Mater.*, 2002, **14**, 1294–1297.
- 103 C. J. Otten, O. R. Lourie, M.-F. Yu, J. M. Cowley, M. J. Dyer, R. S. Ruoff and W. E. Buhro, *J. Am. Chem. Soc.*, 2002, **124**, 4564–4565.
- 104 Y. Zhang, H. Ago, M. Yumura, T. Komatsu, S. Ohshima, K. Uchida and S. Iijima, *Chem. Commun.*, 2002, 2806–2807.
- 105 Y. Wang and X. Duan, *Appl. Phys. Lett.*, 2003, **82**, 272–274.

- 106 T. T. Xu, J.-G. Zheng, N. Wu, A. W. Nicholls, J. R. Roth, D. A. Dikin and R. S. Ruoff, *Nano Lett.*, 2004, **4**, 963–968.
- 107 S. Komatsu and Y. Moriyoshi, *J. Cryst. Growth*, 1990, **102**, 899–907.
- 108 J. Yang, Y. Yang, S. W. Waltermire, X. Wu, H. Zhang, T. Gutu, Y. Jiang, Y. Chen, A. A. Zinn, R. Prasher, T. T. Xu and D. Li, *Nat. Nanotechnol.*, 2012, **7**, 91–95.
- 109 P. Jash and M. Trenary, *J. Phys.: Conf. Ser.*, 2009, **176**, 012011.
- 110 Z. Wang, Y. Shimizu, T. Sasaki, K. Kawaguchi, K. Kimura and N. Koshizaki, *Chem. Phys. Lett.*, 2003, **368**, 663–667.
- 111 K. Kirihara, Z. Wang, K. Kawaguchi, Y. Shimizu, T. Sasaki, N. Koshizaki, K. Soga and K. Kimura, *Appl. Phys. Lett.*, 2005, **86**, 212101.
- 112 H. Ni and X. D. Li, *J. Nano Res.*, 2008, **1**, 10–22.
- 113 J. Xu, Y. Chang, L. Gan, Y. Ma and T. Zhai, *Adv. Sci.*, 2015, **2**, 1500023.
- 114 J. Tian, Z. Xu, C. Shen, F. Liu, N. Xu and H.-J. Gao, *Nanoscale*, 2010, **2**, 1375–1389.
- 115 G. Tai, T. Hu, Y. Zhou, X. Wang, J. Kong, T. Zeng, Y. You and Q. Wang, *Angew. Chem., Int. Ed.*, 2015, **54**, 15473–15477.
- 116 Z. Zhang, A. J. Mannix, Z. Hu, B. Kiraly, N. P. Guisinger, M. C. Hersam and B. I. Yakobson, *Nano Lett.*, 2016, **16**, 6622–6627.
- 117 Z. Zhang, Y. Yang, E. S. Penev and B. I. Yakobson, *Adv. Funct. Mater.*, 2017, **27**, 1605059.
- 118 Q. Zhong, J. Zhang, P. Cheng, B. Feng, W. Li, S. Sheng, H. Li, S. Meng, L. Chen and K. Wu, *J. Phys.: Condens. Matter*, 2017, **29**, 095002.
- 119 M. Q. Le, B. Mortazavi and T. Rabczuk, *Nanotechnology*, 2016, **27**, 445709.
- 120 Y. Jiao, F. Ma, J. Bell, A. Bilic and A. Du, *Angew. Chem., Int. Ed.*, 2016, **55**, 10292–10295.
- 121 H. Wang, Q. Li, Y. Gao, F. Miao, X.-F. Zhou and X. Wan, *New J. Phys.*, 2016, **18**, 073016.
- 122 B. Mortazavi, O. Rahaman, A. Dianat and T. Rabczuk, *Phys. Chem. Chem. Phys.*, 2016, **18**, 27405–27413.
- 123 Z. Pang, X. Qian, R. Yang and Y. Wei, 2016, arXiv preprint arXiv:1602.05370.
- 124 J. Zhao, Z. Yang, N. Wei and L. Kou, *Sci. Rep.*, 2016, **6**, 23233.
- 125 T. Li, *Phys. Rev. B: Condens. Matter Mater. Phys.*, 2012, **85**, 235407.
- 126 Q. Wei and X. Peng, *Appl. Phys. Lett.*, 2014, **104**, 251915.
- 127 Z. Yang, J. Zhao and N. Wei, *Appl. Phys. Lett.*, 2015, **107**, 023107.
- 128 C. Yang, Z. Yu, P. Lu, Y. Liu, H. Ye and T. Gao, *Comput. Mater. Sci.*, 2014, **95**, 420–428.
- 129 E. S. Penev, A. Kutana and B. I. Yakobson, *Nano Lett.*, 2016, **16**, 2522–2526.
- 130 T. Mishonov and E. Penev, *J. Phys.: Condens. Matter*, 2000, **12**, 143.
- 131 Z. Zhang and W. Guo, *Appl. Phys. Lett.*, 2007, **90**, 053114.
- 132 M. Ezawa, *Phys. Rev. B*, 2017, **96**, 035425.
- 133 B. Feng, O. Sugino, R.-Y. Liu, J. Zhang, R. Yukawa, M. Kawamura, T. Iimori, H. Kim, Y. Hasegawa, H. Li, L. Chen, K. Wu, H. Kumigashira, F. Komori, T.-C. Chiang, S. Meng and I. Matsuda, *Phys. Rev. Lett.*, 2017, **118**, 096401.
- 134 G. Profeta, M. Calandra and F. Mauri, *Nat. Phys.*, 2012, **8**, 131–134.
- 135 B. Ludbrook, G. Levy, P. Nigge, M. Zonno, M. Schneider, D. Dvorak, C. Veenstra, S. Zhdanovich, D. Wong, P. Dosanjh, C. Straber, A. Stohr, S. Forti, C. R. Ast, U. Starke and A. Damascelli, *Proc. Natl. Acad. Sci. U. S. A.*, 2015, **112**, 11795–11799.
- 136 Y. Zhao, S. Zeng and J. Ni, *Appl. Phys. Lett.*, 2016, **108**, 242601.
- 137 R. Xiao, D. Shao, W. Lu, H. Lv, J. Li and Y. Sun, *Appl. Phys. Lett.*, 2016, **109**, 122604.
- 138 F. Ma, Y. Jiao, G. Gao, Y. Gu, A. Bilic, Z. Chen and A. Du, *Nano Lett.*, 2016, **16**, 3022–3028.
- 139 X.-L. He, X.-J. Weng, Y. Zhang, Z. Zhao, Z. Wang, B. Xu, A. R. Oganov, Y. Tian, X.-F. Zhou and H.-T. Wang, *FlatChem*, 2017, DOI: 10.1016/j.flatc.2017.07.003.
- 140 X.-F. Zhou, A. R. Oganov, Z. Wang, I. A. Popov, A. I. Boldyrev and H.-T. Wang, *Phys. Rev. B: Condens. Matter Mater. Phys.*, 2016, **93**, 085406.
- 141 Y. Liu, J. Wu, K. P. Hackenberg, J. Zhang, Y. M. Wang, Y. Yang, K. Keyshar, J. Gu, T. Ogitsu, R. Vajtai, J. Lou, P. M. Ajayan, B. C. Wood and B. I. Yakobson, *Nat. Energy*, 2017, **6**, 17127.
- 142 J. E. Padilha, R. H. Miwa and A. Fazzio, *Phys. Chem. Chem. Phys.*, 2016, **18**, 25491–25496.
- 143 X.-F. Zhou and H.-T. Wang, *Adv. Phys.: X*, 2016, **1**, 412–424.
- 144 L.-C. Xu, A. Du and L. Kou, *Phys. Chem. Chem. Phys.*, 2016, **18**, 27284–27289.
- 145 A. Krasheninnikov, P. Lehtinen, A. Foster and R. Nieminen, *Chem. Phys. Lett.*, 2006, **418**, 132–136.
- 146 A. El-Barbary, R. Telling, C. Ewels, M. Heggie and P. Briddon, *Phys. Rev. B: Condens. Matter Mater. Phys.*, 2003, **68**, 144107.
- 147 Z. Zhang, J. Yin, X. Liu, J. Li, J. Zhang and W. Guo, *J. Phys. Chem. Lett.*, 2016, **7**, 867–873.
- 148 L. Tao, E. Cinquanta, D. Chiappe, C. Grazianetti, M. Fanciulli, M. Dubey, A. Molle and D. Akinwande, *Nat. Nanotechnol.*, 2015, **10**, 227–231.
- 149 B. J. Bellott, W. Noh, R. G. Nuzzo and G. S. Girolami, *Chem. Commun.*, 2009, 3214–3215.
- 150 L. Ge, S. Lei, A. H. Hart, G. Gao, H. Jafry, R. Vajtai and P. M. Ajayan, *Nanotechnology*, 2014, **25**, 335701.
- 151 H. Yu, A. Kutana and B. I. Yakobson, *Nano Lett.*, 2016, **16**, 5032–5036.
- 152 X. Liu, Z. Wei, I. Balla, A. J. Mannix, N. P. Guisinger, E. Luijten and M. C. Hersam, *Sci. Adv.*, 2017, **3**, e1602356.
- 153 E. Hwang and S. D. Sarma, *Phys. Rev. B: Condens. Matter Mater. Phys.*, 2007, **75**, 205418.
- 154 L. Ju, B. Geng, J. Horng, C. Girit, M. Martin, Z. Hao, H. A. Bechtel, X. Liang, A. Zettl, Y. R. Shen and F. Wang, *Nat. Nanotechnol.*, 2011, **6**, 630–634.
- 155 V. Bezugly, J. Kunstmann, B. Grundkötter-Stock, T. Frauenheim, T. Niehaus and G. Cuniberti, *ACS Nano*, 2011, **5**, 4997–5005.

- 156 L. Gui-Qin, *Chin. Phys. B*, 2010, **19**, 017201.
- 157 Q. Zhong, L. Kong, J. Gou, W. Li, S. Sheng, S. Yang, P. Cheng, H. Li, K. Wu and L. Chen, *Phys. Rev. Mater.*, 2017, **1**, 021001(R).
- 158 M. Liu, V. I. Artyukhov and B. I. Yakobson, *J. Am. Chem. Soc.*, 2017, **139**, 2111–2117.
- 159 See Research Highlights in: *Nature*, 2017, **542**, 141.
- 160 S. I. Er, G. A. de Wijs and G. Brocks, *J. Phys. Chem. C*, 2009, **113**, 18962–18967.
- 161 T. B. Tai and M. T. Nguyen, *Chem. – Eur. J.*, 2013, **19**, 2942–2946.
- 162 X. Zhang, J. Hu, Y. Cheng, H. Y. Yang, Y. Yao and S. A. Yang, *Nanoscale*, 2016, **8**, 15340–15347.
- 163 H. Jiang, Z. Lu, M. Wu, F. Ciucci and T. Zhao, *Nano Energy*, 2016, **23**, 97–104.
- 164 B. Mortazavi, A. Dianat, O. Rahaman, G. Cuniberti and T. Rabczuk, *J. Power Sources*, 2016, **329**, 456–461.
- 165 Y. Zhang, Z.-F. Wu, P.-F. Gao, S.-L. Zhang and Y.-H. Wen, *ACS Appl. Mater. Interfaces*, 2016, **8**, 22175–22181.
- 166 J. Dai, Y. Zhao, X. Wu, J. Yang and X. C. Zeng, *J. Phys. Chem. Lett.*, 2013, **4**, 561–567.
- 167 X. Luo, J. Yang, H. Liu, X. Wu, Y. Wang, Y. Ma, S.-H. Wei, X. Gong and H. Xiang, *J. Am. Chem. Soc.*, 2011, **133**, 16285–16290.
- 168 X. Wu, Y. Pei and X. C. Zeng, *Nano Lett.*, 2009, **9**, 1577–1582.
- 169 Z. Zhu, X. Cai, C. Niu, C. Wang and Y. Jia, *Appl. Phys. Lett.*, 2016, **109**, 153107.
- 170 P. Zhang and V. H. Crespi, *Phys. Rev. Lett.*, 2002, **89**, 056403.
- 171 L. Zhang, Z. Wang, S. Du, H.-J. Gao and F. Liu, *Phys. Rev. B: Condens. Matter Mater. Phys.*, 2014, **90**, 161402.
- 172 Y. Mu, F. Ding and H. Lu, *RSC Adv.*, 2015, **5**, 11392–11396.
- 173 H. Zhang, Y. Li, J. Hou, K. Tu and Z. Chen, *J. Am. Chem. Soc.*, 2016, **138**, 5644–5651.
- 174 H. Zhang, Y. Li, J. Hou, A. Du and Z. Chen, *Nano Lett.*, 2016, **16**, 6124–6129.
- 175 J. Yang, S. Song, S. Du, H.-J. Gao and B. I. Yakobson, *J. Phys. Chem. Lett.*, 2017, **8**, 4594–4599.
- 176 *Materials Genome Initiative*, <https://www.mgi.gov>, 2016.